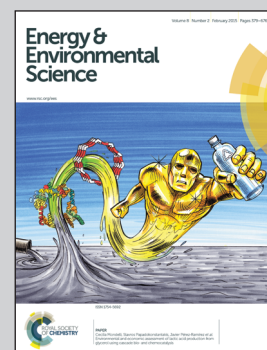


Showcasing research from Prof. Ziqi Liang's group from Fudan University, Shanghai, China.

Title: Solution processed organic thermoelectrics: towards flexible thermoelectric modules

Organic semiconductor materials have advantages of low cost, light weight, mechanical flexibility and low-temperature solution processability over large areas, enabling the development of personal, portable, and flexible thermal modules.

As featured in:



See Ziqi Liang et al.,  
*Energy Environ. Sci.*, 2015, **8**, 401.

## REVIEW

Cite this: *Energy Environ. Sci.*, 2015, 8, 401Solution processed organic thermoelectrics:  
towards flexible thermoelectric modules

Yani Chen, Yan Zhao and Ziqi Liang\*

Organic semiconductor materials have advantages of low cost, light weight, mechanical flexibility and low-temperature solution processability over large areas, enabling the development of personal, portable, and flexible thermal modules. This review article summarizes the recent progress made in the area of organic thermoelectrics (TEs), including organic molecular structures, devices, characterization methods, and approaches to improve the performance. We begin with the discussion of each TE parameter and particularly their correlations in organic TEs. Then the TE applications of molecular organic semiconductors, poly(3,4-ethylenedioxythiophene), polymer nanostructures and molecular junctions are reviewed. Next we turn to highlight the nanocomposites of polymers and carbon nanotubes or nanocrystals, which lead to enhanced TEs. Interestingly, the merging of TEs and photovoltaics offers a new direction towards a great capability of electric energy output. Critical challenges of organic TE materials include stability, sample preparation and measurement techniques, which are also discussed. Finally, the relationships among organic semiconductor structures, hybrid composites, doping states, film morphology and TE performance are revealed, and a viable avenue is envisioned for synergistic optimization of organic TEs.

Received 17th October 2014  
Accepted 7th November 2014

DOI: 10.1039/c4ee03297g

www.rsc.org/ees

## Broader context

Thermoelectric (TE) energy conversion is considered as an effective means to directly harvest electricity from heat. Thus, TE materials are attractive for application in waste heat recovery and solar thermal utilization. However, traditional high-performance inorganic TE materials are based on rare elements and hence lack scalability of production. Recently, organic TE materials have sparked great interest owing to their unique advantages over inorganic counterparts, offering the potential of high-throughput production of flexible thermal modules. The TE performance is characterized by  $zT = S^2\sigma T/\kappa$ , where  $z$  is the figure of merit,  $T$  is the temperature,  $S$  is the Seebeck coefficient,  $\sigma$  is the electrical conductivity, and  $\kappa$  is the thermal conductivity. Intrinsically low  $\kappa$  values of organic TE materials are desirable, yet there remains a trade-off between  $\sigma$  and  $S$ . This review article summarizes the recent advances in the area of organic TEs, aiming to unveil the relationship among molecular structures of organic semiconductors, doping states, film morphology of nanocomposites and TE properties.

## 1. Introduction

Thermoelectric (TE) materials can directly transform waste heat from automobile exhaust systems or excess solar thermal flux into usable electrical power.<sup>1–4</sup> TEs are not only technically simple and reliable but also environmentally friendly; therefore, TEs have long been recognized as a highly promising transformative technology to reduce global energy consumption.

A suitable TE material must be good at conducting electricity yet poor at conducting heat. The TE performance is characterized by a dimensionless

$$zT = \frac{S^2\sigma T}{\kappa} \quad (1.1)$$

where  $z$  is the figure of merit,  $T$  is the temperature (K),  $S$  is the thermopower or Seebeck coefficient (voltage per unit

temperature difference,  $\text{V K}^{-1}$ ),  $\sigma$  is the electrical conductivity ( $\text{S m}^{-1}$ ), and  $\kappa$  is the thermal conductivity ( $\text{W m}^{-1} \text{K}^{-1}$ ). Among those parameters,  $S^2\sigma$  ( $\text{W m}^{-1} \text{K}^{-2}$ ) is often defined as a power factor. It is however hard to achieve a high  $zT$  in traditional bulk materials because all of these TE parameters are highly correlated, which poses the challenges of simultaneously enhancing electrical conductivity and thermopower while also lowering thermal conductivity.<sup>5–8</sup> The maximum conversion efficiency ( $\eta$ ) of a TE material depends on its Carnot efficiency and TE properties ( $S$ ,  $\sigma$  and  $\kappa$ ). In a thermoelectric generator (TEG), the efficiency  $\eta$  is often expressed by:<sup>9</sup>

$$\eta = \frac{T_h - T_c}{T_h} \frac{\sqrt{1 + zT_m} - 1}{\sqrt{1 + zT_m} + T_c/T_h} \quad (1.2)$$

where  $T_m = (T_h + T_c)/2$ , and  $T_h$  and  $T_c$  are the temperatures of the hot and the cold side of the device, respectively.

There have been recently tremendous advances in conventional inorganic TE materials,<sup>10–16</sup> which however have drawbacks such as high cost of production, scarcity of materials,

Department of Materials Science, Fudan University, Shanghai 200433, China. E-mail: zqliang@fudan.edu.cn

toxicity as well as limited scope of applications. To overcome these intrinsic issues, research on organic TE materials as alternatives has emerged. Significant progress has been made in the past few years for organic material based thermoelectrics, in particular organic/inorganic nanocomposites have shown great potential of further enhancing  $zT$ .<sup>17–20</sup> Owing to their unique advantages of low cost, light weight, low-temperature solution processing over a large area compared to inorganic counterparts, together with intrinsically low thermal conductivity and high Seebeck coefficient, organic semiconductors are considered as a promising class of TE materials, allowing for the development of personal, portable, and flexible thermoelectric modules.<sup>21–23</sup>

Unique to organic semiconductors is enabling the rational design and synthesis of molecular structures, tunable band structures, and controllable doping treatments, all of which render them ideal candidates for TE applications. The TE properties of organic semiconductors are however known to be

coupled with each other and in particular conducting polymers are known for their morphological complexity and anisotropy in thin films. Thus, optimization of  $zT$  in conducting polymers requires a systematic understanding of the influences of chemical and electronic structures along with solid-state morphology on electrical conductivity, thermal conductivity and Seebeck coefficient. Fortunately, the structure–charge transport relationship of conducting polymers, which has been extensively investigated in organic electronics, would in turn help understanding of various origins of electrical conductivity and the Seebeck effect in conducting polymers in order to attain high power factors. To realize the above goals, reliable and systematic methods for organic thermoelectric property characterization are highly required.

This review article is organized as follows. Firstly, an overview of TEs is presented by covering several important aspects—phonons in thermal transport, charge carriers—holes and electrons—in electrical transport, the Seebeck effect, and intimate correlation of those steps. Second, we discuss the organic semiconductors in TEs including general issues of each thermoelectric parameter, molecular organic semiconductors, poly(3,4-ethylenedioxythiophene) (PEDOT), polymer nanostructures and molecular junctions. Third, we turn to nanocomposites of polymers and carbon nanotubes or nanocrystals, which offer an effective method for enhanced TEs. Next and interestingly, the merging of TEs and photovoltaics (PVs) opens up a new direction. Still, organic TE materials are challenged by several critical issues such as stability, sample preparation and measurement techniques, which are also discussed. Finally, a conclusion is made particularly with regard to the relationship between organic semiconductors and TE performance, and a perspective for



*Yani Chen graduated with a B.S. in Textile Engineering from Donghua University in 2013. She is currently a Ph.D. candidate in the Department of Materials Science at Fudan University under the supervision of Professor Ziqi Liang. Her research areas focus on organic photovoltaics and organic thermoelectrics.*



*Yan Zhao graduated with a B.S. in Materials Science and Engineering from Jiangsu University in 2013. She is currently a Masters student in Department of Materials Science at Fudan University under the supervision of Professor Ziqi Liang. Her research areas center on metal alloy based thermoelectrics.*



*Ziqi Liang obtained his Ph.D. in Polymer Science at the Department of Materials Science and Engineering from The Pennsylvania State University in May 2006. Then he pursued the postdoctoral work at University of Cambridge from May 2006–May 2008. In June 2008, he joined National Research Energy Laboratory as a postdoctoral researcher and was later promoted to Scientist III. In July 2012, Dr Liang moved back to China and joined Department of Materials Science at Fudan University as a professor. Currently, Prof. Liang's group conducts the research encompassing (i)  $\pi$ -conjugated polymers – design, synthesis, function, and devices, (ii) conducting polymer nanostructures, (iii) optoelectronics – organic solar cells, light-emitting diodes and their interface and charge transport studies, (iv) thermoelectrics – organic semiconductors and organic–inorganic nanocomposites for thermal-to-electrical energy conversion.*

optimization and construction of flexible organic TE modules is given correspondingly.

## 2. Organic semiconductors in TEs

### 2.1 General issues

Organic TE materials are potentially abundant. The majority of organic TE materials in the literature are based on  $\pi$ -conjugated polymers (or conducting polymers) such as polyaniline, polyacetylene, polypyrrole, polythiophene, polyphenylene, and PEDOT as well as small molecules such as pentacene, fullerene, tetrathiafulvalene (TTF) and 2,3,5,6-tetrafluoro-7,7,8,8-tetracyanoquinodimethane (F<sub>4</sub>TCNQ). Molecular structures of these representative organic TE materials are shown in Table 1.

The development of organic TE materials has just begun and yet the efficiency is mainly restricted by the relatively low power factor in comparison to that of inorganic materials. One major hurdle—similar to their inorganic counterparts—is that the enhancement of electrical conductivity *via* doping chemistry is often accompanied by the resulting low Seebeck coefficient. It is therefore crucial to balance the electrical conductivity and the Seebeck coefficient, thereby maximizing the power factor and  $zT$ . Thus far, a range of conducting polymers as shown in Table 1 have been tested for their TE performance with a variety of dopants such as I<sub>2</sub>, camphor sulfonic acid (CSA), and FeCl<sub>3</sub>. The concept of optimizing the power factor of conducting polymers using electrochemical doping has also proved as a versatile tool, allowing for the control and measurement of the oxidation

level. Electrical conductivity is related to electronic charge  $q$  ( $1.6 \times 10^{-19}$  C), free carrier density  $p_f$  ( $\text{cm}^{-3}$ ) and charge carrier mobility  $\mu$  ( $\text{cm}^2 \text{V}^{-1} \text{s}^{-1}$ ) as

$$\sigma = qp_f\mu \quad (2.1)$$

Typically, for organic semiconductors  $\sigma$  is  $\sim 10^{-4}$  S  $\text{m}^{-1}$ ,  $p_f$  is  $\sim 10^{16}$   $\text{cm}^{-3}$  and  $\mu$  is  $\sim 10^{-4}$   $\text{cm}^2 \text{V}^{-1} \text{s}^{-1}$  as seen from the following reviewed literature. The doping processes (both chemical and electrochemical treatments) are directly related to the variation of  $p_f$ .

$$p_f = \frac{N}{V} = \frac{nN_A}{V} = \frac{m_0N_A}{MV} = \frac{mw\%N_A}{MV} = \frac{\rho w\%N_A}{M} \quad (2.2)$$

where  $m$  is the mass of the solution,  $m_0$  is the mass of dopants,  $p_f$  is the carrier concentration,  $N$  is the number of dopant molecules,  $V$  is the volume of the solution,  $n$  is the molar number of dopant molecules,  $M$  is the molar mass,  $N_A$  is Avogadro's constant ( $6.02214129 \times 10^{23}$   $\text{mol}^{-1}$ ),  $w\%$  is the mass fraction of dopant molecules or the doping level, and  $\rho$  is the density of the solution. Tunable molecular structures of organic semiconductors can be acquired through synthetic chemistry, which has a great impact on intrinsic  $\mu$ . However, the charge mobility is largely undermined by doping. Thus, it is necessary to take all these factors into consideration to make tradeoff and reach remarkable TE performances.

The conduction mechanism in organic TE materials, especially the conducting polymer, is quite different from that of inorganic materials and therefore very important for the

Table 1 Molecular structures of representative organic TE materials

| Polymers       | Chemical structure | Small molecules     | Chemical structure |
|----------------|--------------------|---------------------|--------------------|
| Polyaniline    |                    | Pentacene           |                    |
| Polyacetylene  |                    | TTF                 |                    |
| Polypyrrole    |                    | F <sub>4</sub> TCNQ |                    |
| Polythiophenes |                    | C60                 |                    |
| Polyphenylene  |                    |                     |                    |
| PEDOT          |                    |                     |                    |

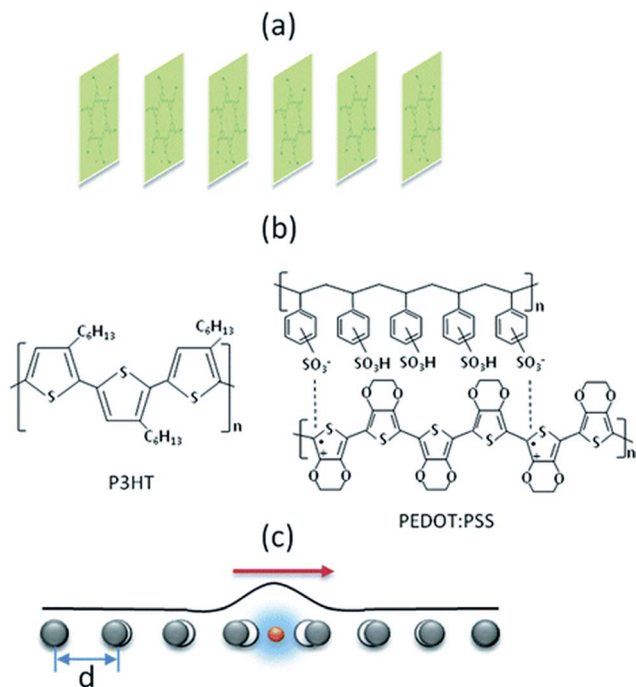


Fig. 1 (a) Quasi-1D self-assembled molecular NWs that are composed of 1D stacks of planar building blocks loosely held together by van der Waals or  $\pi$ - $\pi$  interactions. (b) 1D single molecular chains of conducting polymers. (c) Schematic of the small-polaron transport model to describe the thermoelectric transport in organic materials shown in panels a and b. The strong electron-phonon interaction in these organic materials causes lattice distortions around the electron. The electron is trapped by the polarized field formed itself. Reprinted with permission from ref. 24. Copyright 2011 The American Chemical Society.

optimization of TE properties. The conduction in conducting polymers occurs *via* the polaron/bipolaron formation due to the strong carrier lattice coupling. As shown in Fig. 1, a small-polaron model was used to describe such a strong interaction of electron and phonon in organic materials.<sup>24</sup> The strong electron-phonon interaction causes lattice distortion around the electron which moves along the chain but is also trapped by the polarized field formed itself. Each monomer unit of the conducting polymer can be viewed as a site. Electrical transport arises from the polarons hopping from one site to another caused by overlap of the electron wave functions on adjacent sites, where the intersite coupling is essential for TE properties.

The Seebeck coefficient, a defining parameter for thermoelectric materials, depends on the contributions to the conductivity of charge carriers at energies away from the Fermi level ( $E_F$ ).<sup>9,25</sup> According to the Mott relationship for degenerate semiconductors,  $S$  is defined as:

$$S = \frac{\pi^2 k_B^2 T}{3q} \left( \frac{d \ln \sigma(E)}{dE} \right) \Big|_{E=E_F} \quad (2.3)$$

where  $k_B$  is the Boltzmann constant ( $1.38 \times 10^{-23} \text{ J K}^{-1}$ ) and  $E$  is the electron energy (eV). For nondegenerate semiconductors the Seebeck coefficient is given by the Boltzmann equation:

$$S = \frac{k_B}{q} \left[ \frac{(E - E_F)}{k_B T} + A \right] \quad (2.4)$$

where  $A$  is the heat of transport constant for motion over extended states in ordinary semiconductors ( $A \cong 1$ ) or for the hopping of carriers in materials with localized states. Normally, highly conductive materials tend to exhibit the conductivity from carriers close to the  $E_F$ . Eqn (2.4) suggests that the doping level will determine the position of  $E_F$  and hence the magnitude of the TE power generation. High doping levels will push  $E_F$  into the conduction band due to the increased carrier concentration. This subsequently causes the number of electronic states above and below  $E_F$  to be more equivalent, negatively reducing  $S$ . Thus it is necessary to maximize the electrical conductivity—as long as the thermal conductivity retains a phononic contribution while somewhat maintaining unequal distributions in the density-of-states (DoS).

On the other hand, many recent  $zT$  improvements in organic TE materials originated from thermal conductivity, similar to those of conventional inorganic TE materials. As for organic TE materials, the thermal conductivity value is typically below  $1 \text{ W m}^{-1} \text{ K}^{-1}$  as seen from this review article, approaching the lowest limit of thermal conductivity of inorganic TE materials. The thermal conductivity is defined by the relationship of  $\kappa = C_p \rho \alpha$  ( $\text{W m}^{-1} \text{ K}^{-1}$ ) where  $C_p$  is the specific heat capacity ( $\text{J kg}^{-1} \text{ K}^{-1}$ ),  $\rho$  is the density ( $\text{kg m}^{-3}$ ) and  $\alpha$  is the thermal diffusivity ( $\text{m}^2 \text{ s}^{-1}$ ).<sup>9,25</sup> The thermal conductivity is also described by

$$\kappa = \kappa_L + \kappa_e \quad (2.5)$$

where  $\kappa_L$  corresponds to lattice or phonon contribution and  $\kappa_e$  relates to electron contribution. For the phonon contribution, it is expressed as

$$\kappa_L = \frac{1}{3} c v l \quad (2.6)$$

where  $c$  is the heat capacity per unit volume ( $\text{J K}^{-1} \text{ m}^{-3}$ ),  $v$  is the sound velocity ( $\text{m s}^{-1}$ ),  $l$  is the phonon mean free path (m). The sound velocity is usually in the range of  $10^3$ – $10^4 \text{ m s}^{-1}$  in polymers. Specifically, the values of sound velocity for typical conducting polymers—PEDOT:PSS and poly(3-hexylthiophene) (P3HT)—are  $1.58 \times 10^3$  and  $2.87 \times 10^3 \text{ m s}^{-1}$ , respectively.<sup>26,27</sup> For organic polymers,  $\kappa_L$  is low and often lies in the range of  $0.1$ – $1.0 \text{ W m}^{-1} \text{ K}^{-1}$ , and more importantly  $\kappa_L$  is independent of the doping level. Enormous studies have shown that point defects from doping, nanostructuring, and heterostructures or alloys which create rich hetero-interfaces and grain boundaries can cause phonon scattering, thus decreasing  $\kappa_L$ . For the electron contribution, one can assume the ideal electron gas model, following the Wiedemann-Franz law:<sup>9,25</sup>

$$\kappa_e = L \sigma T \quad (2.7)$$

where  $L$  is the Lorentz number. Note that organic semiconductors do not typically obey the Wiedemann-Franz law due to strong charge lattice coupling. The Lorentz factor  $L = (\pi^2/3) (k_B/e)^2 \approx 3.29 (k_B/e)^2$  in the law can be thus modified to  $L \approx$

$(0.44-1) (k_B/e)^2$  for typical conducting polymers.<sup>24</sup> The coefficient ranging from 0.44 to 1 depends on the materials and the doping level. This modification is based upon the Holstein model for the small-polaron system, which considers strong charge lattice coupling. For organic semiconductors, given the typical electrical conductivity of  $\sim 10^{-4} \text{ S m}^{-1}$ ,  $\kappa_e$  can be estimated to be *ca.*  $10^{-10} \text{ W m}^{-1} \text{ K}^{-1}$  which is totally negligible compared to  $\kappa_L$ . As a consequence, the thermal conductivity in organic TE materials is most likely independent of the doping level and is probably dominated by phonons. It is likely that only when electrical conductivities a few orders of magnitude higher are reached will electron-mediated thermal conductivity become important.<sup>28</sup>

## 2.2 Molecular organic semiconductors

As mentioned before, one advantage of organic semiconductors used as TE materials is the facile tunability of their chemical and physical properties through simple modifications of their molecular structure to reach the optimum TE performance. Such structural modifications have been found to greatly impact the charge transport such as electrical conductivity and charge mobility in conjugated polymers. For instance, a very early attempt on polymer TEs originated from the work of Leclerc *et al.*, in which a series of as-synthesized alternating poly(2,7-carbazole) derivatives were doped with  $\text{FeCl}_3$  and their TE properties as a function of the doping level were evaluated.<sup>29</sup> One polycarbazole derivative in the study—poly[*N*-9'-heptadecan-yl-2,7-carbazole-*alt*-5,5'-(4',7'-di-2-thienyl-2',1',3'-benzothiadiazole)] (PCDTBT)—exhibited a high electrical conductivity of up to  $500 \text{ S cm}^{-1}$  and a relatively high Seebeck coefficient of up to  $70 \mu\text{V K}^{-1}$ , leading to a maximum power factor value of  $19 \mu\text{W m}^{-1} \text{ K}^{-2}$ , superior to that of benchmark polyaniline (PANI) ( $\sim 0.4 \mu\text{W m}^{-1} \text{ K}^{-2}$ ). The high electrical conductivity was obtained by introducing a secondary alkyl side-chain on the carbazole unit and packing units such as benzene and benzothiadiazole units along the conjugated backbone. These strong interchain interactions facilitated the transport of the charge carriers through the polymeric structure.

Katz *et al.* successfully demonstrated that intentional DoS inhomogeneities in organic-based compositions can be designed to simultaneously increase the Seebeck coefficient and conductivity.<sup>30</sup> A polymer blend of P3HT and poly(3-hexylthiophene) (P3HTT) that differed only slightly in oxidation potential was proposed. It should be noted that those blends that have larger differences in oxidation potentials could even define more precisely tailored DoS profiles through the use of three or more oxidizable species. The ground-state hole carriers of the poly(alkylthiophene) blends were created by doping a minor additive component—2,3,5,6-tetrafluoro-7,7,8,8-tetracyanoquinodimethane ( $\text{F}_4\text{TCNQ}$ ), and remained mainly at an orbital energy set below the hole energy of the major component of the blend. Besides, electron-carrying semiconductor mixtures can be used to provide the companion n-type semiconductor side of a module as shown in Fig. 2. In both cases, controlled doping can define the  $E_F$  to have an arbitrary offset from the energy level of the high-mobility component in the blend. In

stark contrast to other TE systems, doping in this regard would not greatly alter the  $E_F$ . Electrical transport, however, was expected to occur through the major component, leading to a regime in which the hole conductivity and Seebeck coefficient may be increased in parallel. In short, this work demonstrated a route for designing TE materials in which increases of both Seebeck coefficient and conductivity do not compromise each other. Yet there is ultimately a trade-off between introducing thermal activation in the conductivity, which increases  $S$ , and having the energy barrier between the ground state and conducting charge carriers being so great that conductivity is unlikely, lowering  $\sigma$ .

The Katz group later found a surprising negative Seebeck coefficient for the pristine tetrathiafulvalene (TTF)-modified thiophene copolymer, which is attributed to the strong hole trapping activity of the TTF group.<sup>31</sup> At first, the pristine thiophene polymer was observed to show an increase in the Seebeck coefficient when initially doped with  $\text{F}_4\text{TCNQ}$ . Among them, the Seebeck coefficient value was found to be positive  $75 \mu\text{V K}^{-1}$  with 8 wt% of  $\text{F}_4\text{TCNQ}$ , as a low-lying hole state was presumably filled. Further increasing the dopant concentration decreased the Seebeck coefficient, as expected. In contrast, the TTF-functionalized thiophene copolymer displayed the negative Seebeck coefficient, which was unexpected. The reason is that, holes being so thoroughly trapped by TTF and thus electrons in the highest occupied TTF orbitals could be excited on heating into impurity states that dominate the Seebeck coefficient. Even if this occurred to a very small degree and there were no mobile holes present, a negative Seebeck coefficient would result. Once a sufficient amount of dopants were added, the material became hole-dominated again, and the Seebeck coefficient reverted to a positive sign. While the conductivity was increased with the dopant level, the power factor remained low ( $< 0.2 \mu\text{W m}^{-1} \text{ K}^{-2}$ ) because of the high concentration of TTF traps and general disorder in the polymer. Much more ordered polymers, and possibly lower-lying principal orbitals for holes, would be needed to realize useful power factors from TTF addition.

An n-type TE couple is highly needed for practical TE applications, yet n-type organic semiconductors are largely scarce due to their synthetic difficulty and poor air-stability. However, recent advances in n-type organic TE materials are encouraging. For example, Chabinye *et al.* demonstrated that n-type conducting polymer poly[*N,N'*-bis(2-octyl-dodecyl)-1,4,5,8-naphthalenedicarboximide-2,6-diyl]-*alt*-5,5'(2,2'-bithiophene)] (P(NDIOD-T2)) is a promising candidate for organic TEs *via* n-type doping.<sup>32</sup> Through two n-type dopants—dihydro-1*H*-benzimidazol-2-yl (*N*-DMBI) and 4-(1,3-dimethyl-2,3-dihydro-1*H*-benzimidazol-2-yl)-*N,N*-diphenylaniline (*N*-DPBI), the electrical conductivity of P(NDIOD-T2) was increased up to  $\sim 10^{-3} \text{ S cm}^{-1}$ . TEM imaging of these two doped polymer structures revealed the highly ordered structure of the *N*-DMBI doped P(NDIOD-T2) through its film thickness. Owing to their poor solubility in P(NDIOD-T2), however, very few dopants were electrically active (*i.e.*, only one out of one hundred dopant molecules) in the mixture solution, which was estimated to ultimately contribute a mobile electron to the conduction band of the polymer. As a

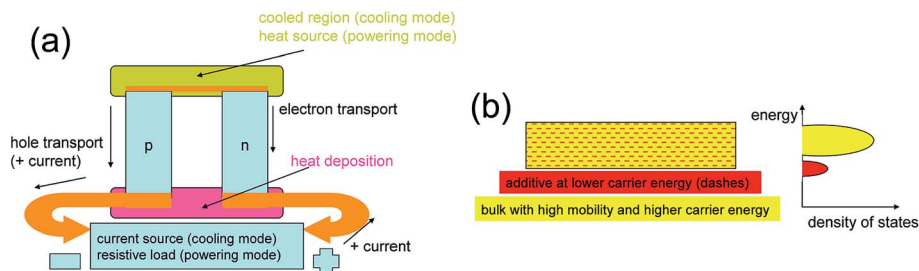


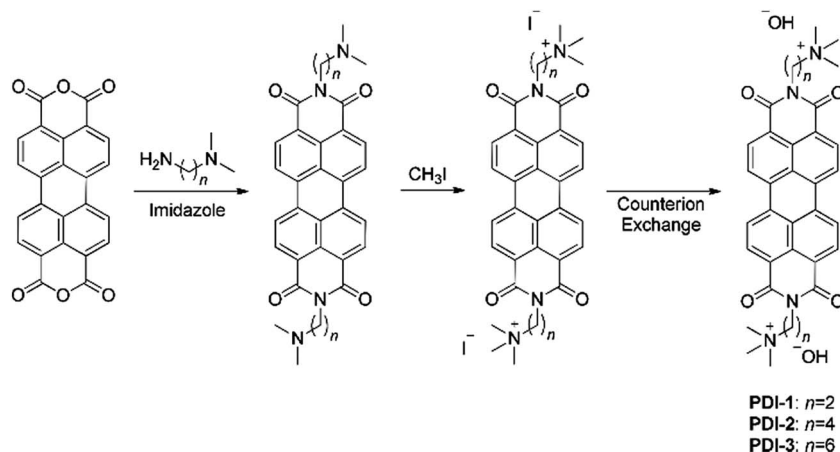
Fig. 2 (a) Layout and current paths of a thermoelectric module based on one p–n semiconductor couple. (b) Schematic of the proposed organic thermoelectric composite, consisting of an additive that sets the Fermi level and a bulk in which charge carriers at higher energy levels are transported. Reprinted with permission from ref. 30. Copyright 2010 The American Chemical Society.

result, the dopant molecules aggregated on the top surface, leaving the polymer morphology largely unchanged. Despite the phase segregation of dopants, P(NDIOD-T2) exhibited comparable Seebeck coefficient and power factor to p-type polymers with similar conductivities. It was envisioned that rational engineering of dopant-polymer miscibility would afford greatly improved TE performance.

The single p–n TE couple was very recently constructed based on newly developed n-type and p-type organic TE materials, both of which have low thermal conductivities, high electrical conductivities, and reasonable Seebeck coefficients.<sup>33</sup> Two n-types of poly[Na<sub>x</sub>(Ni-ett)] and poly[K<sub>x</sub>(Ni-ett)], along with one p-type of poly[Cu<sub>x</sub>(Cu-ett)], were measured with temperature dependent TE performances. These two n-type materials exhibited high *zT* values of 0.1–0.2 around 400 K, among the highest for organic materials. The TE module composed of 35 n–p couples was made, which was able to output a voltage of 0.26 V, a current of 10.1 mA, and a power of 2.8  $\mu\text{W cm}^{-2}$ —among the highest for organic TE devices ever reported under a temperature bias of  $\Delta T = 80$  K. More importantly, the module showed very good stability and hence its potential of functioning as a TE refrigerator.

A new concept of self-doping was more recently employed for both n-type and p-type organic TE research. Segalman and

coworkers reported the way of coupling molecular design of a perylene diimide (PDI) platform with an effective self-doping mechanism.<sup>34</sup> The electronic properties were achieved by changing the alkyl spacer length between the charged side groups and the PDI backbone of such PDI small molecules in Scheme 1. For example, increasing the length of the alkyl chain from two to six methylene groups enhances the electrical conductivity 100-fold, while the Seebeck coefficient was negative (indicating n-type electronic transport) and remained approximately constant with spacer length, both collectively boosting the power factor by two orders of magnitude. Nevertheless, much work is needed to probe the effect of changes in the alkyl spacer on structural and TE properties and to gain a deep understanding of the self-doping mechanism. Similarly, in a most recent report by Bazan and coworkers, engineering of ionic side chains of conjugated polyelectrolytes (CPEs) has been proved to be an effective method to tune the electrical properties.<sup>35</sup> A series of anionic narrow band gap self-doped CPEs with  $\pi$ -conjugated cyclopenta-[2,1-*b*:3,4-*b'*]-dithiophene-*alt*-4,7-(2,1,3-benzothiadiazole) backbones have been designed and synthesized with different counterions (Na<sup>+</sup>, K<sup>+</sup>, vs. tetrabutylammonium, TBA) and lengths of alkyl chains (C4 vs. C3). These materials were readily doped to provide air-stable, water-soluble conductive materials. The CPE structures which have smaller



Scheme 1 Chemical structures of PDI small molecules with varying alkyl length (*n*) between the PDI backbone and the charged side group. Reprinted with permission from ref. 34. Copyright 2013 Wiley-VCH.

counterions and shorter side chains exhibited a higher doping level and thus higher electrical conductivities with lower Seebeck coefficient, thereby leading to a higher power factor. Meanwhile, these CPEs formed more ordered films and hence tighter  $\pi$ - $\pi$  stacking and better crystallinity. The CPE-C3-Na showed  $0.22 \pm 0.02 \text{ S cm}^{-1}$ ,  $195 \pm 5 \mu\text{V K}^{-1}$ , and thus  $0.84 \mu\text{W m}^{-1} \text{K}^{-2}$ . Of special note, chemical modifications of the pendant side chains do not influence the out-of-plane thermal conductivity.

To increase the carrier mobility of organic TE semiconductors is regarded as the most viable route to improving the power factor. Recent progress in organic electronics with the design of novel conducting polymer structures has led to intrinsically high carrier mobility achieved at definite energy levels. Zhu *et al.* reported a series of high-mobility polymeric semiconductors used for TEs.<sup>36</sup> Two benchmark donor-acceptor (D-A) copolymers—poly[[4,4'-bis(2-ethylhexyl)dithieno[3,2-*b*:2',3'-*d*]silole)-2,6-diyl-*alt*-(2,1,3-benzothiadiazole)-4,7-diyl] (PSBTBT) and poly[[2,5-bis(2-hexyldecyl)-2,3,5,6-tetrahydro-3,6-dioxopyrrolo[3,4-*c*]pyrrole-1,4-diyl]-*alt*-[[2,2':5',2''-terthiophene]-5,5''-diyl]] (PDPP3T), together with two benchmark conducting polymers—P3HT and poly(2,5-bis(3-dodecylthiophen-2-yl)thieno[3,2-*b*]thiophene) (PBTBT) were chemically doped by simply dipping the polymer films into dopant solution, thus obtaining high electrical conductivities. Additionally, temperature-dependent measurements of electrical conductivity and Seebeck coefficient were carried out to understand the transport mechanisms and energetic distribution of charge carrier DoS. As a result, bulk mobilities of these four chemically doped polymers were extracted, and the positive temperature dependence of Seebeck coefficients was analyzed in order to clarify the origins of the disparity in their TE properties. Comparisons were then made as follows. The doping ratio in terms of charges per sulfur atom can be extrapolated from XPS spectra. Using the bulk density of polymer repeat units and doping ratios, the density of charge carriers ( $\text{cm}^{-3}$ ) can be roughly estimated according to eqn (2.2). Upon high doping, all polymers give a free carrier concentration above  $10^{20} \text{ cm}^{-3}$ . At such high doping levels, the power factor values of PDPP3T, PSBTBT, and PBTBT were optimized, in which the Seebeck coefficient increased with temperature, reaching 25, 3.5, and  $14 \mu\text{W m}^{-1} \text{K}^{-2}$ , respectively, at 320 K. The inferior TE property of PSBTBT was suggested to arise from the disordering in molecular stacking and microstructures by energy-independent scattering of electrical carriers. In contrast, heavily doped PBTBT had the highest mobility of  $1.6 \text{ cm}^2 \text{V}^{-1} \text{s}^{-1}$  and the lowest Seebeck coefficient, presumably due to the smaller DoS with undesirable profile around  $E_F$  at a high doping level, which is in part attributed to the long interdigitated alkyl side chains.

Often, doping of organic semiconductors increases the charge density and yet reduces their mobility, making it challenging to improve the TE performance. Clearly, there has to be a compromise between charge density and mobility upon doping. In a recent theoretical study, Shuai and coworkers proposed a simple model to quantitatively obtain the optimal doping level and the  $zT$  peak value from the intrinsic carrier mobility, the lattice thermal conductivity, and the effective DoS

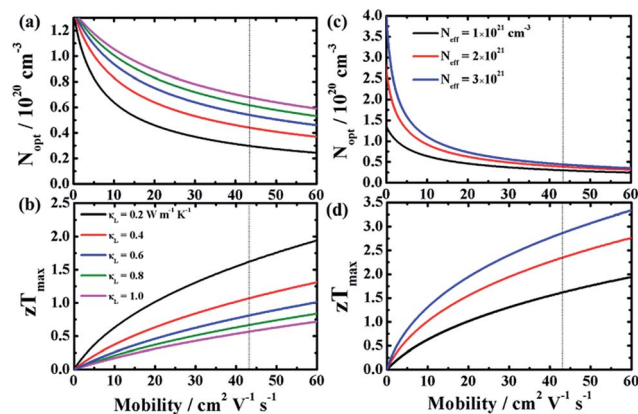


Fig. 3 Dependence of (a) the optimal carrier concentration and (b) the corresponding maximum value of  $zT$  on the carrier mobility and the lattice thermal conductivity with the effective DoS fixed at  $N_{\text{eff}} = 10^{21} \text{ cm}^{-3}$  at room temperature. Dependence of (c) the optimal carrier concentration and (d) the corresponding maximum value of  $zT$  on the carrier mobility and the effective DoS  $N_{\text{eff}}$  with the lattice thermal conductivity fixed at  $\kappa_L = 0.2 \text{ W m}^{-1} \text{K}^{-1}$  at room temperature. Reprinted with permission from ref. 37. Copyright 2014 The American Chemical Society.

( $N_{\text{eff}}$ ).<sup>37</sup> Assuming that the effective DoS is fixed, it can be deduced that a high intrinsic mobility and a low lattice thermal conductivity will lead to a low optimal carrier concentration. Quantitatively, as shown in Fig. 3, the optimal doping level and the corresponding peak value of  $zT$  were plotted as a function of the intrinsic carrier mobility, the lattice thermal conductivity, and the effective DoS at room temperature. The intrinsic mobility and the effective DoS are related to the electronic structure of a material, and the lattice thermal conductivity is related to the lattice vibration. The model reveals that high intrinsic mobility and low lattice thermal conductivity give rise to a low optimal doping level and a high maximum  $zT$  value. These findings would guide one in the search of new organic TE materials and their optimization.

Attention should be paid to the morphology of conducting polymers, which would greatly impact the charge carrier mobility. Yang and coworkers have recently built bulk interpenetrating networks (IPNs) of conjugated polymer—poly(3-butylthiophene) (P3BT) nanowires in an insulating polystyrene supporting matrix.<sup>38</sup> This way led to effectively decreased thermal conductivity and increased electrical conductivity, as compared to the neat conjugated polymer, without compromising the Seebeck coefficient, and ultimately enhanced  $zT$  value. A key reason for such improvements is the quasi-1D charge transport in the bulk IPNs, which caused a higher electric conductivity and a smaller activation energy than neat P3BT. An additional benefit from the bulk IPNs is lower cost, optical transparency and flexibility.

### 2.3 PEDOT

PEDOT is the most widely used conductive polymer because of its high conductivity, good stability, and remarkable capabilities of easy doping and solution processing. PEDOT when

doped with PSS is routinely used as a hole-transporting layer in organic light-emitting and photovoltaic devices. Another unique feature of PEDOT is its intrinsically low thermal conductivity. These advantages make PEDOT attractive for developing organic-based high-performance TE materials. PEDOT has been chemically or electrochemically doped to control the charge density and electrical conductivity while without significantly compromising the Seebeck coefficient, thus achieving the improved TE properties.

PEDOT with high electrical conductivity upon doping with several counter-ions such as  $\text{ClO}_4$ ,  $\text{PF}_6$  and bis(trifluoromethylsulfonyl)imide (BTfMSI) was prepared using electropolymerization on gold.<sup>39</sup> After removing the gold layer, a very thin semiconducting polymer film can be isolated. The increase in electrical conductivity with the change of the counter-ion is mainly due to the stretching of the polymer chains. By changing the size of counter-ions, the conductivity of PEDOT was increased by a factor of three while the Seebeck coefficient remained at the same order of magnitude. Also, the conductivity decreased with the reduction time while the Seebeck coefficient increased. The best TE efficiency has been observed in PEDOT:BTfMSI, in which a power factor of  $147 \mu\text{W m}^{-1} \text{K}^{-2}$  and thermal conductivity of  $0.19 \text{ W m}^{-1} \text{K}^{-1}$  were obtained, resulting in a  $zT$  of  $\sim 0.22$  at room temperature. To increase the electrical conductivity of conducting polymers, oxidants and mediators for the solution casting polymerization can be finely controlled.<sup>40</sup> For instance, highly conductive PEDOT films with high uniformity and large area accessibility were prepared using a mixture of pyridine and poly(ethylene glycol)-*block*-poly(propylene glycol)-*b*-poly(ethylene glycol) tri-block copolymer (PEPG) as mediators for the polymerization of 3,4-ethylenedioxythiophene (EDOT) in the presence of Fe-tosylate (Tos). The resulting PP-PEDOT showed an electrical conductivity of  $1355 \text{ S cm}^{-1}$  at an oxidation level of

24.1%. Further, by precisely controlling the oxidation level of PEDOT electrochemically (*e.g.*, reduced at 0.1 V), a maximum power factor of  $1270 \mu\text{W m}^{-1} \text{K}^{-2}$  was obtained. The flexible TE generator was achieved by coating a PP-PEDOT film on PET substrates (Fig. 4). Such thin thermoelectrics could be bent, folded, and cut by scissors and used to generate electricity by the touch of fingertips as shown in Fig. 4.

If its doping level is controlled precisely, a conducting polymer can achieve both low thermal and high electrical conductivities, yet the Seebeck coefficient usually decreases when the electrical conductivity increases. Crispin and coworkers have accurately controlled the oxidation level in PEDOT combined with its low intrinsic thermal conductivity ( $\sim 0.37 \text{ W m}^{-1} \text{K}^{-1}$ ), yielding  $zT = 0.25$  at room temperature.<sup>41,42</sup> After an extensive oxidation doping process with Tos—switching the color of PEDOT from a dark blue to a light blue-grey, PEDOT exhibited very high electrical conductivities up to  $1000 \text{ S cm}^{-1}$ , while the Seebeck coefficient was so low that the  $zT$  remained about  $10^{-2}$ – $10^{-3}$ . To resolve this issue of low  $zT$ , Crispin's team slightly de-doped and partially reduced the fully oxidized PEDOT—using tetrakis(dimethylamino)ethylene (TDAE) to maximize the Seebeck coefficient as well as the electrical conductivity.

It is however difficult to precisely control those chemical doping processes, partly because the measurement of the exact oxidation level is not straightforward, and also the choice of counterions is limited. Therefore, an electrochemical doping process was demonstrated by the Crispin team as a versatile tool of optimizing the TE power factor of conducting polymers. In their work, the researchers controlled electrically the TE properties of PEDOT doped with PSS by varying the gate voltage.<sup>43</sup> Electrochemical doping facilitates the control and measurement of the oxidation level *via* tuning of the electrode potential

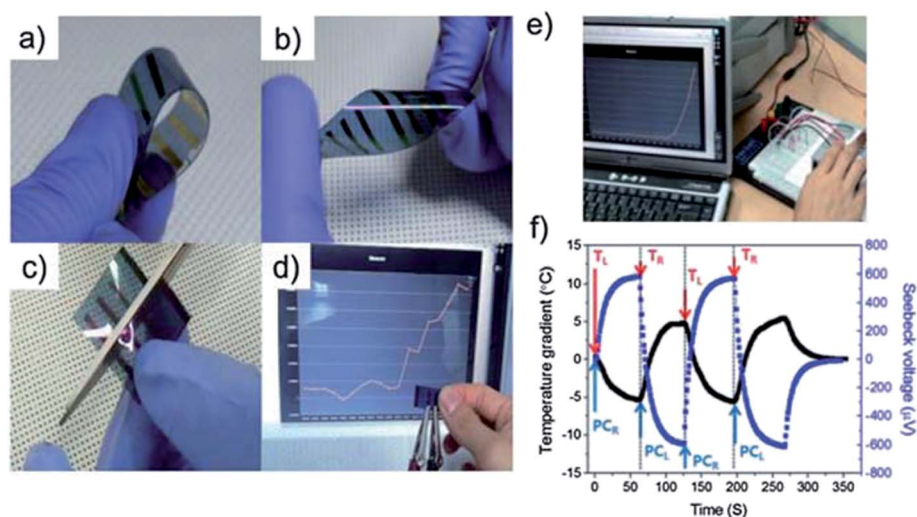


Fig. 4 Photographic images and electricity generation by the touch of fingertips of the flexible PP-PEDOT thermoelectric film. (a) Bending, (b) twisting, and (c) cutting with scissors images of PP-PEDOT films. (d) Electricity generation by fingertip touch at one side with air and (e) a Peltier module reference. (f) Electricity generation (blue squares) and the corresponding temperature gradient (black squares) measured from (e). (TL: touch left side, TR: touch right side with fingertips, PCR: a right side Peltier device cooling, and PCL: a left side Peltier device cooling to generate the temperature difference). Reprinted with permission from ref. 40. Copyright 2013 The Royal Society of Chemistry.

while enabling the measurement of the charging currents. Moreover, many counterions are available to balance the doping charges along the polymer chains simply by adding different salts in the electrolyte. This work has provided clear experimental evidence that further optimization of the TE properties of conducting polymers will require better knowledge of the details of the DoS close to  $E_F$ , including the effects of disorder and the nature of the charge carriers, as indicated in Fig. 5. It would be expected that good TE polymers might be those with sharp DoS at  $E_F$ , and hence a first strategy would be to reduce the disorder. This method provides an easy tool to study the physics behind the TE properties while optimizing the polymer TE performance.

Furthermore, the Crispin team lately reported the transformation of semiconducting polymers as semi-metallic.<sup>44,45</sup> Semi-metals, exemplified by bismuth, graphite and telluride alloys, are suitable for TE applications in that they have no energy bandgap and a very low DoS at the  $E_F$ , and typically have a higher Seebeck coefficient and lower thermal conductivities compared with metals. As shown in Fig. 6, through creating a network of bipolarons which initiated the transition from a Fermi glass to a semi-metal, the electrical conductivity of PEDOT was enhanced and correspondingly a marked increase was observed in the Seebeck coefficient. The high Seebeck value, the metallic conductivity at room temperature and the absence of unpaired electron spins together make polymer semi-metals attractive for both TEs and spintronics.

The dedoping method mentioned above was also used for treatment of PEDOT:PSS nanofilms by over-coating a mixture of dimethyl sulfoxide (DMSO) and hydrazine (HZ), a strong chemical reducing agent, to enhance the TE properties.<sup>46</sup> This over-coating step led to molecular reorganization of PEDOT:PSS nanofilms by removal of excess PSS chains and formation of neutral states of PEDOT chains. Such conformational changes resulted in an improvement in the Seebeck coefficient from 30 to 142  $\mu\text{V K}^{-1}$ , and a decrease in the electrical conductivity from 726 to 2  $\text{S cm}^{-1}$ . By controlling the concentration of HZ, an optimized power factor of 112  $\mu\text{W m}^{-1} \text{K}^{-2}$  was obtained with 0.0175 wt% of HZ in DMSO at room temperature. The corresponding electrical conductivity and Seebeck coefficient under

optimized conditions were 578  $\text{S cm}^{-1}$  and 67  $\mu\text{V K}^{-1}$ , respectively.

As equally important as control of the doping level to maximize  $zT$  is reducing the dopant volume in organic semiconductors, as found by Pipe *et al.*<sup>47</sup> By minimizing the total dopant volume, all three parameters constituting  $zT$  varied were simultaneously improved so that  $zT$  increased. This stands in sharp contrast to inorganic semiconductors, for which these parameters have trade-offs. Using in-plane values for both power factor and thermal conductivity, maximum  $zT$  values of 0.42 and 0.28 were obtained for DMSO and ethylene glycol (EG) mixed PEDOT:PSS, respectively, at room temperature.

In addition, a multilayered structure was found to improve the electrical conductivity by the quantum effect.<sup>48</sup> Specifically, a pure organic PEDOT:PSS nanofilm was used as a working electrode to electrodeposit polymer films of polythiophene (PTh) and its derivatives in a boron trifluoride diethyl ether (BFEE) solution, fabricating a novel generation of three bilayered nanofilms. The electrical conductivities of these PEDOT:PSS/PTh, PEDOT:PSS/poly(3-methylthiophene) (P3MeT), and PEDOT:PSS/P3HT nanofilms reached 123.9, 136.5, and 200.5  $\text{S cm}^{-1}$ , respectively. These three bilayered nanofilms displayed good electrochemical stability and enhanced TE performances. The temperature dependences of TE parameters in a range of 300–100 K were studied. The electrical conductivities of all the three samples decreased with the decreasing temperature, indicating a semiconductor behavior. Seebeck coefficients were positive at room temperature, suggesting the presence of holes as majority carriers, and decreased with the decreasing temperature. At 300 K, PEDOT:PSS/PTh nanofilms exhibited a power factor of 1.57  $\mu\text{W m}^{-1} \text{K}^{-2}$ , whereas those of PEDOT:PSS/P3MeT and PEDOT:PSS/P3HT were 4.43 and 5.79  $\mu\text{W m}^{-1} \text{K}^{-2}$ , respectively.

It is worth noting that organic semiconductors have a preferred molecular orientation during the film formation, which could produce an anisotropic film. Anisotropic TE properties of benchmark PEDOT:PSS films, for instance, in the in-plane and through-plane directions have been studied.<sup>49</sup> It was found that the PEDOT:PSS films had highly anisotropic carrier transport properties and thermal conductivity. The

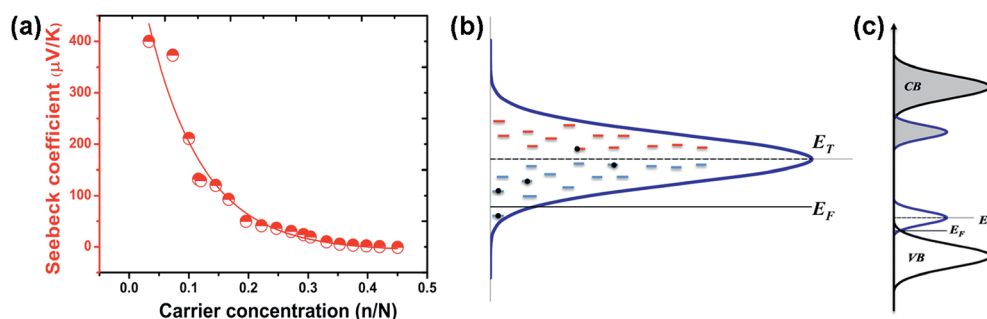


Fig. 5 (a) Seebeck coefficient of electrochemically doped PEDOT:PSS as a function of fractional charge carrier concentration. The experimental results suggest exponential growth of the Seebeck coefficient upon polymer electrochemical reduction. (b) Gaussian DoS with localized states below  $E_T$ . (c) Conduction band (CB) and valence band (VB) with localized bands formed by polarons/bipolarons at the forbidden energy gap. Reprinted with permission from ref. 43. Copyright 2012 The American Chemical Society.

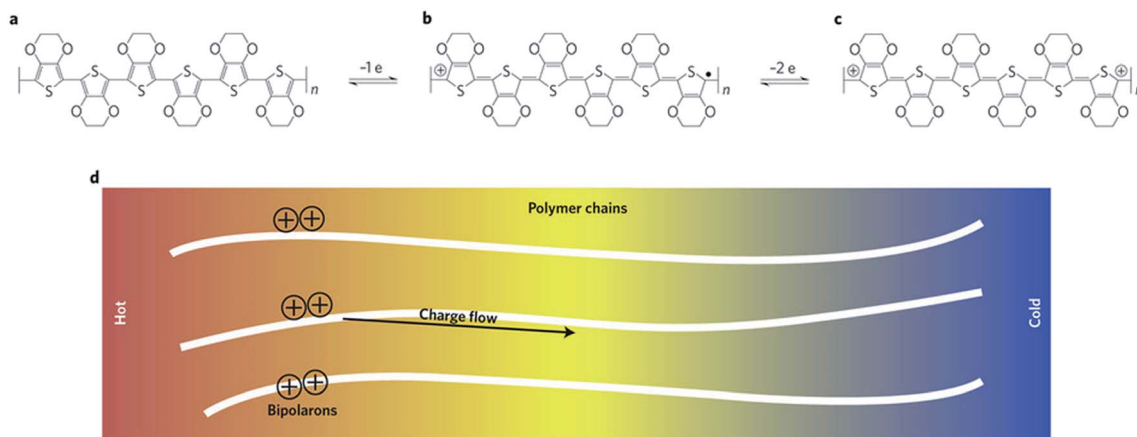


Fig. 6 Charge carriers in PEDOT. (a) In the neutral form, each repeat unit is best represented by the aromatic form with two double bonds. (b) Removal of one electron leads to a singly charged polaron; a positive charge that induces a rearrangement of the double bonds in the repeat units. The plus symbol is the positive charge and the dot is a radical (unpaired electron). (c) Removal of another electron leads to a bipolaron having two positive charges delocalized along the backbone. (d) The bipolarons move in a thermal gradient to form an electrical potential in PEDOT:Tos. Reprinted with permission from ref. 45. Copyright 2014 Nature Publishing Group.

anisotropic carrier transport properties can be explained by the lamellar structure of the PEDOT:PSS films where the PEDOT nanocrystals could be isolated by the insulating PSS in the through-plane direction. The anisotropic thermal conductivity was mainly attributed to the lattice contribution from PSS because the polymer chain was oriented along the substrate. The use of small molecule dopants along with the control of the crystal orientation could be an effective strategy for optimizing the TE performance.

#### 2.4 Polymeric nanostructures

As its dimensions decrease, the TE properties of a material would undergo remarkable changes.<sup>9,25</sup> One-dimensional (1D) nanostructures such as nanowires, nanotubes or nanofibers have been recently utilized for TE applications. For instance, a notably high power factor was obtained in quasi-1D self-assembled organic molecular nanowires based on a rigorous theoretical evaluation, indicating that the use of low-dimensional structures can indeed be a promising direction to achieve high TE performance.

Yang *et al.* theoretically studied the TE properties (*i.e.*, electrical conductivity, Seebeck coefficient, and power factor) of those quasi-1D self-assembled molecular nanowires (NWs) based on a rigorous evaluation of the Kubo formula using the Holstein model.<sup>24</sup> The molecular NWs were composed of either 1D conducting polymer chains, coupled by covalent bonds, or linear stacks of planar building blocks, held together by van der Waals or  $\pi$ - $\pi$  interactions. These 1D molecular NWs are expected to be excellent TE materials because (i) the thermal conductivity along the stacking direction can be very small due to interfacial phonon scattering and (ii) the Seebeck coefficient could be very large due to the narrow and sharp DoS. The authors then systematically studied the dependence of TE properties on a variety of physical parameters, including intersite coupling, electron-phonon interaction, chemical potential

(doping concentration), and temperature. It was found that the TE properties were strongly affected by the intersite coupling and the dielectric constant. If the phonon thermal conductivity is assumed to be  $0.2 \text{ W m}^{-1} \text{ K}^{-1}$ , the  $zT$  value of a molecular NW theoretically can reach 15.2. The model was further applied to study the TE properties of 1D polymer chains of P3HT and PEDOT:PSS. The power factor can reach  $0.05 \text{ W m}^{-1} \text{ K}^{-2}$  for a PEDOT:PSS chain. This study indicates that low-dimensional conducting polymers could be promising high- $zT$  TE materials.

As one experimental example, enhanced TE properties were observed in ultra-long electrodeposited PEDOT nanowires.<sup>50</sup> These NWs were prepared by electropolymerizing EDOT in aqueous  $\text{LiClO}_4$  within a template prepared using the lithographically patterned nanowire electrodeposition process. These nanowires were 40–90 nm in thickness, 150–580 nm in width, and 200  $\mu\text{m}$  in length. The electrical conductivity and Seebeck coefficient were measured from 190 K to 310 K by fabricating heaters and thermocouples on top of arrays of 750 PEDOT nanowires. As shown in Fig. 7,  $S$  increased in direct proportion to  $T$  for both PEDOT thin films and nanowires, which is in accord with the predictions of the following Mott equation:

$$S = \frac{\pi^2 k_B^2 m^* T}{(3\pi^2)^{2/3} \hbar q \nu_f^2} \quad (2.8)$$

where  $\hbar$  is Planck constant and  $m^*$  is the effective mass of majority carriers. Due to the lower carrier concentrations, such PEDOT nanowire arrays consistently produced higher  $S$  values than those for PEDOT films, that is, up to  $-122 \mu\text{V K}^{-1}$  for nanowires and  $-57 \mu\text{V K}^{-1}$  for films at 310 K. Interestingly, the PEDOT nanowires also had a higher electrical conductivity than neat films, because electron mobility was greater in nanowires by a factor of 3. As a result, power factors up to  $9.2 \times 10^{-5} \text{ W m}^{-1} \text{ K}^{-2}$  was obtained.

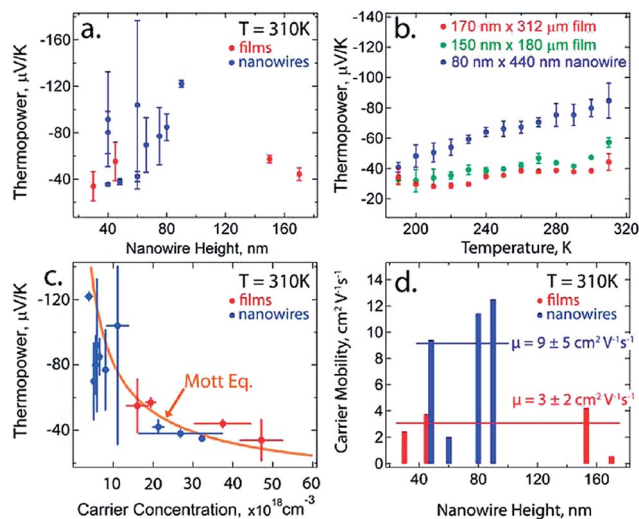


Fig. 7 (a) Measured  $S$  versus nanowire height for PEDOT nanowires and films at 310 K. (b)  $S$  versus temperature over the range from 190 K to 310 K. Error bars represent  $1\sigma$  for 2–4 measurements at each temperature point. (c)  $S$  versus carrier concentration fitted with the Mott relationship (eqn (2.8)). (d) Electron mobilities versus the film or nanowire height, showing also (horizontal line) the mean mobility value. Reprinted with permission from ref. 50. Copyright 2011 The American Chemical Society.

Nevertheless, theory of Yang *et al.* on 1D conducting polymers<sup>24</sup> was unable to apply to the insulating polymers. For example, recent investigations on polymer nanofibers showed extraordinarily high thermal conductivities, which spurred much interest in thermally conductive polymers. High-modulus polymer fibers were recently studied to advance an understanding of the mechanisms for thermal transport in 1D fibers.<sup>51</sup> Among the high modulus fibers as examined, liquid crystalline polybenzobisoxazole (PBO) fibers were found to have the highest thermal conductivity of  $20 \text{ W m}^{-1} \text{ K}^{-1}$  at room temperature, surpassing the conductivity of highly crystalline polyethylene. For both fiber types, thermal conductivity near room temperature scaled with temperature, suggesting an intrinsic limit to the thermal conductivity governed by anharmonicity, not structural disorder. Because of the high degree of elastic anisotropy, longitudinal acoustic phonons at a direction along the fiber axis are most likely to dominate the thermal transport in PBO. Higher thermal conductivities might be possible if the molecular structure or polymer morphology can be modified to increase the lifetimes of the high-frequency longitudinal acoustic modes that propagate along the rigid polymer chain.

Another example suggested that individual chains of polyethylene (PE)—the simplest and most widely used polymer—can have extremely high thermal conductivity.<sup>52</sup> Practical applications of these polymers may also require that the individual chains form fibers or films. In this respect, high-quality ultra-drawn PE nanofibers were fabricated with diameters of 50–500 nm and lengths up to tens of millimeters. A comparison between micrometer and nanometer sized fibers was made that the thermal conductivity generally increased with increasing

draw ratios where the thermal conductivity of microfibers saturated when the draw ratio was above 100 while that of nanofibers did not show saturation, indicating that there is still room for enhancement. The thermal conductivity of the nanofibers was found to be as high as  $\sim 104 \text{ W m}^{-1} \text{ K}^{-1}$ , which is larger than the conductivities of about half of the pure metals. The high thermal conductivity is attributed to the restructuring of the polymer chains by stretching, which improves the fiber quality toward an ‘ideal’ single crystalline fiber.

Opposing influences of 1D nanostructures on thermal conductivity can be seen in the above two types of examples— $\pi$ -conjugated molecular nanowires and nonconjugated crystalline nanofibers. Possible explanations are as follows. In the  $\pi$ -conjugated nanowires, phonon transport occurred along the  $\pi$ -conjugated backbone and between the  $\pi$ -stacks, in the latter of which interfacial phonon scattering decreased the thermal conductivity. By contrast, in the nonconjugated nanofibers, reduced entanglements through remarkable stretching of polymer chains in the anisotropic direction decreased phonon scattering and thus largely increased the thermal conductivity. Apparently, more work is needed to gain a better understanding of the origins of thermal conductivity in low-dimensional conducting nanostructures in comparison to that of insulating polymers.

## 2.5 Molecular junctions

The strong coupling effect of electrical and thermal conductivity (eqn (2.7)) is known to be detrimental to increasing the Seebeck coefficient. Physically, the magnitude and sign of the Seebeck coefficient can be approximately understood as the amount of entropy “dragged along” by the flow of charge inside a material; in other words, it is the entropy per unit charge in the material.<sup>9</sup> A high thermal conductivity will reduce the entropy difference, which is the driving force for charge transport under thermal diffusion, through the electron–phonon interaction between the hot and cold regions. A favorable combination of high electrical conductivity yet low thermal conductivity has been recently realized in hybrid metal–polymer–metal molecular junctions, where the ohmic metal–polymer contacts allow for the formation of good electrical conductivity while the phonon scattering at metal–polymer interfaces minimizes the thermal conductivity.

Segalman, Majumdar and coworkers at UC Berkeley for the first time studied thermoelectricity in small molecule based thin film devices.<sup>53</sup> Molecular junctions were formed by trapping molecules between two gold electrodes and then the Seebeck coefficient was obtained by measuring the voltage-generated across them when a temperature bias was imposed difference across the junction. Such metal/molecule/metal heterojunctions can provide the transport through either the highest occupied molecular orbital (HOMO) and lowest unoccupied molecular orbital (LUMO) energy levels while having very low vibrational heat conductance. As a result, the junction Seebeck coefficients of 1,4-benzenedithiol (BDT), 4,4'-dibenzene-dithiol (DBDT), and 4,4''-tribenzenedithiol (TBDT) were measured at room temperature to be  $8.7 \pm 2.1$ ,  $12.9 \pm 2.2$ , and

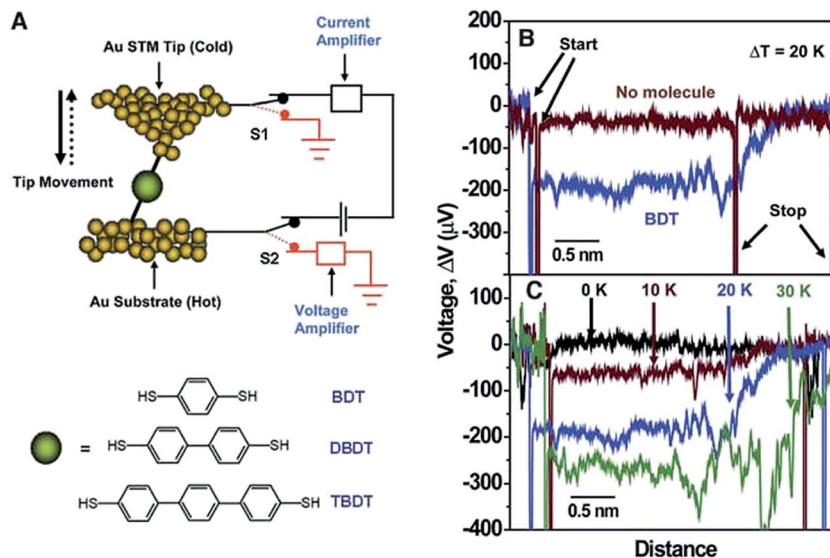


Fig. 8 (A) Schematic description of the experimental setup based on an STM break junction. Molecules of BDT, DBDT, or TBDT are trapped between the Au STM tip kept at ambient temperature and a heated Au substrate kept at temperature  $\Delta T$  above the ambient temperature. When the tip approaches the substrate, a voltage bias is applied and the current is monitored to estimate the conductance. When the conductance reaches a threshold of  $0.1 G_0$ , the voltage bias and the current amplifier are disconnected. A voltage amplifier is then used to measure the induced thermoelectric voltage,  $\Delta V$ , and the tip is gradually pulled away from the substrate. (B) A plot of the thermoelectric voltage measured as a function of the tip-sample distance when a temperature differential  $\Delta T = 20$  K is applied (Au tip at ambient temperature and substrate at ambient temperature + 20 K). The blue curve is obtained when an Au-BDT-Au junction is broken. The red curve shows a control experiment performed on a clean gold substrate. (C) Typical thermoelectric voltage traces for tip-substrate temperature differentials of 0, 10, 20, and 30 K for Au-BDT-Au junctions. Reprinted with permission from ref. 53. Copyright 2007 American Association for the Advancement of Science.

$14.2 \pm 3.2 \mu\text{V K}^{-1}$ , respectively, as shown in Fig. 8. The positive sign unambiguously indicates hole conduction in these heterojunctions, whereas the  $E_F$  position of Au for Au-BDT-Au junctions was identified to be 1.2 eV above the HOMO energy level of BDT. The ability to study thermoelectricity in molecular junctions provides the opportunity to address the fundamental questions about their electronic structure and to begin exploring molecular TE energy conversion.

The Berkeley team further studied thermoelectricity in fullerene (*i.e.*, C60, [6,6]-phenyl-C61-butyric acid methyl ester (PCBM), and C70)-metal molecular heterojunctions in which a single-molecule was trapped between metal electrodes (*i.e.*, Pt, Au, Ag) to understand transport properties at organic-inorganic interfaces.<sup>54</sup> Electronic transport in these systems can be described by the Landauer formalism, where charge carriers transmit between opposite electrodes, through a molecular bridge. The transport was highly dependent on the energy level alignment between the molecular orbitals and the  $E_F$  (or work function) of the metal contacts. To date, the majority of single-molecule measurements have focused on simple small molecules where transport is dominated through the HOMO energy level. In these systems, energy level alignment was limited by the absence of electrode materials with low  $E_F$ s (*i.e.*, large work functions). Alternatively, more controllable alignment between molecular orbitals and the  $E_F$  can be achieved with molecules whose transport is dominated by the LUMO because of readily available metals with lower work functions. Fullerene junctions in this study demonstrated the first strongly negative (n-type) molecular thermopower corresponding to transport through

the LUMO, which achieved the remarkably high thermopower of  $-33 \mu\text{V K}^{-1}$  in comparison to an Au-Au junction thermopower of  $\sim 2 \mu\text{V K}^{-1}$  or BDT thermopower of  $\sim 8 \mu\text{V K}^{-1}$ . While the electronic conductance of fullerenes was highly variable, due to the multiple orientations and electrode coupling of molecules between the junctions, the thermopower showed predictable trends based on the alignment of the LUMO with the work function of the electrodes. Both the magnitude and trend of the thermopower suggested that heterostructuring organic and inorganic materials at the nanoscale can further enhance the TE performance, thereby providing a new pathway for designing TE materials. This work also suggested that organic dopants at inorganic interfaces can lead to further enhancements of TE efficiency.

As such, Lee *et al.* lately performed TE measurements of BDT and C60 molecules with Ni and Au electrodes using a home-built scanning tunneling microscope.<sup>55</sup> The thermopower of C60 was negative for both Ni and Au electrodes, indicating the transport of carriers through the LUMO energy level in both cases, as expected from the work functions. The Au-BDT-Au junctions exhibited a positive thermopower, yet the Ni-BDT-Ni junctions surprisingly exhibited a negative thermopower, due to the strong spin hybridization of the HOMO level at  $E_F$  of BDT coupled with s- and d-states of the ferromagnetic Ni electrode according to first-principles calculations. This work demonstrated the tuning of the thermopower of molecular junctions using the spin degrees of freedom.

Polymer based molecular junctions for TE applications have also been studied.<sup>56</sup> For instance, Hu *et al.* fabricated a hybrid

metal/polymer/metal thin-film device to obtain a large Seebeck effect by using high-electrical conducting metals and low-thermal conducting polymers.<sup>57</sup> This was demonstrated with p-type doped conducting polymer—polypyrrole and photovoltaic polymer blend—P3HT:PCBM composite. Such hybrid device structures exhibited strong electrical conduction yet weak thermal conduction, as schematically indicated in Fig. 9. For the electrical conduction in such metal/polymer/metal thin-film devices, the ohmic metal/polymer interface together with a p-type doped polymer film allowed the holes to transport through the HOMO energy level in the polymer film. However, the doped polymer film functioned as a bottleneck to limit thermal conduction in the entire devices. The metal/polymer interface further reduced the thermal conduction through two possible mechanisms—acoustic mismatch due to different phonon densities and velocities, and phonon scattering due to interface imperfections and boundaries.

Furthermore, PEDOT:PSS was used in a hybrid metal/polymer/metal thin film design and achieved a high Seebeck coefficient of  $252 \mu\text{V K}^{-1}$  on a relatively low temperature scale.<sup>58</sup> The polymer film thickness was varied in order to investigate its influences on the Seebeck effect. (i) The observed high Seebeck effect indicated that the metal/polymer/metal design can develop a large entropy difference in internal energy of charge carriers between high and low-temperature metal electrodes under a temperature difference. This large entropy difference can lead to a sufficient electrical potential for the development of significant Seebeck effect due to charge transport through ohmic Al/PEDOT:PSS interfaces and bulk PEDOT:PSS film. (ii) On the other hand, the low thermal conductivity of the bulk PEDOT:PSS film along with phonon scattering at Al/PEDOT:PSS interfaces

formed a bottleneck to limit the thermal conduction from a high to low-temperature metal electrode in the Al/PEDOT:PSS/Al device. This limited thermal conduction maintained the entropy difference between high and low-temperature metal electrodes towards the development of the Seebeck effect. Therefore, the Al/PEDOT:PSS/Al device can exhibit a significant Seebeck effect. The temperature-dependent Seebeck coefficient suggested that increasing temperature can largely boost electrical conduction through charge density but still limited thermal conduction through interfacial phonon scattering in the Al/PEDOT:PSS/Al device. As a consequence, a high Seebeck effect can be developed at a high temperature. (iii) In addition, changing polymer film thickness can vary the Seebeck coefficient in the Al/PEDOT:PSS/Al device through surface and bulk electron-phonon coupling. Clearly, the hybrid metal/polymer/metal thin-film design showed an effective structure to combine high-electrical conducting inorganic metals and low-thermal conducting polymers for the development of efficient Seebeck devices.

Moreover, a poly(2-methoxy-5-(2'-ethylhexyloxy)-*p*-phenylene vinylene) (MEH-PPV) based multilayer was used in such hybrid thin-film structure, in which photoexcitation can lead to a large Seebeck coefficient of  $305 \mu\text{V K}^{-1}$  under the light intensity of  $16 \text{ mW cm}^{-2}$ .<sup>59</sup> Upon light illumination, the electrical conductivity was increased by one order of magnitude to  $8.2 \times 10^{-5} \text{ S cm}^{-1}$  because of the increased charge density through the dissociation of photogenerated excited states. Therefore, photoexcitation led to a simultaneous increase on electrical conductivity and Seebeck coefficient in excited states among these ITO/MEH-PPV/Au devices, in sharp contrast to that induced by doping—increasing electrical conductivity but decreasing Seebeck coefficient.

### 3. Organic-based nanocomposites for TEs

Recently, organic-based nanocomposites have become the central focus of developing the next generation TE materials in that it is possible to enhance the electrical conductivity while significantly reducing the thermal conductivity in such bulk nanocomposites.<sup>19,20</sup> Two main physical mechanisms account for the TE performance enhancements of nanocomposites: (1) the nanoscale grain size or inclusion which enhances phonon-boundary scattering even at elevated temperatures, and (2) the energy filtering effect of charge carriers at the boundary and/or *via* enhanced ionized impurity scattering at the organic/inorganic interfaces, both of which strongly scatter the heat phonons and thus largely decrease the lattice thermal conductivity of nanocomposites and increase the power factor. Note that the Fermi level of each component of the composite has to match each other in order to avoid unnecessary energy barrier. As a result, recent advances in TE nanocomposites exhibited remarkable performances and also showed great promise of printing large-area, flexible TE modules.

#### 3.1 Polymer/carbon nanotube composites

The limitation of low  $zT$  values in TE nanocomposites was attempted by employing the computational modelling to

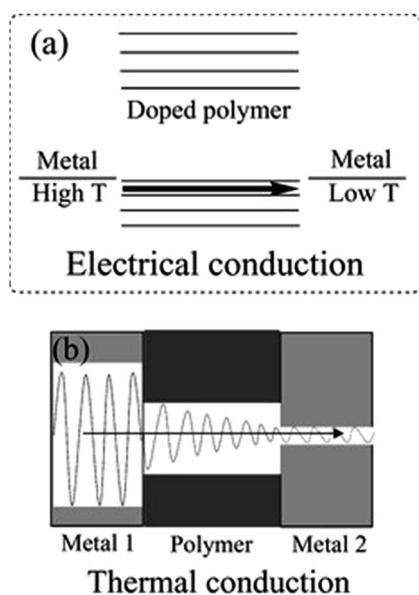


Fig. 9 (a) Electronic levels to indicate allowed charge transport in the hybrid metal/polymer/metal thin-film device. (b) Schematic thermal transport to indicate limited thermal conduction in the hybrid metal/polymer/metal thin-film device. Reprinted with permission from ref. 57. Copyright 2011 Wiley-VCH.

accelerate the selection of suitable pairs of conductive polymers and inorganic TE materials.<sup>19,20</sup> For instance, researchers have recently worked on the improvement of electrical conductivity of a variety of polymers by incorporating carbon nanotubes (CNTs) in the polymer matrix with different methods. CNTs were found to give improved conductivity and mechanical strength to the polymer matrix. On the other hand, coating the CNTs with a thin polymer layer to enhance the size-dependent energy-filtering effect and to increase the carrier mobility can simultaneously enhance the electrical conductivity and Seebeck coefficient of the composites. It is however critical to homogeneously disperse and obtain a good interfacial connection between the polymer and CNTs to maximize desired properties. In this respect, an *in situ* interfacial polymerization seems to be a good method for uniform dispersion.

Carbon nanotubes—either single-walled (SW) or multi-walled (MW)—can be used to p-doped P3HT and the resulting composites displayed an encouraging TE performance.<sup>60</sup> A maximum power factor value of  $\sim 6 \pm 2 \mu\text{W m}^{-1} \text{K}^{-2}$  in P3HT:MWCNT composites was estimated for the MWCNT composition of 10–40 wt%. In contrast, a power factor value of  $25 \pm 6 \mu\text{W m}^{-1} \text{K}^{-2}$  was found in P3HT:SWCNT composites for the SWCNT composition at only 8 wt% and moreover a maximum power factor value of  $\sim 95 \pm 12 \mu\text{W m}^{-1} \text{K}^{-2}$  at 42–81 wt%. The reason is that SWCNTs consistently resulted in a higher electrical conductivity with a maximum value above  $10^3 \text{ S cm}^{-1}$ ; more importantly, thermal conductivities of composites of 8–10 wt% contents of SWCNTs did not compromise low bulk thermal conductivity of the P3HT matrix, which are still comparable to that of reference P3HT (*ca.*  $0.19 \pm 0.05 \text{ W m}^{-1} \text{K}^{-1}$ ) and thus promised a high  $zT > 10^{-2}$  at room-temperature. All P3HT:CNT composites can be readily prepared on plastic substrates, emphasizing their suitability for large-area, flexible TE applications.

Likewise, composites of SWCNTs and PANI were prepared, exhibiting abnormally enhanced TE transport properties.<sup>61</sup> Such hybrid films were prepared by casting the suspension containing well-dispersed SWCNTs and camphor sulfonic acid (CSA)-doped PANI. With the increasing SWCNT content, the electrical conductivity of the hybrid film first increased and then decreased, while the Seebeck coefficient increased monotonically in the present SWCNT content range. At 64 wt% SWCNT, the electrical conductivity reached the maximum value of  $769 \text{ S cm}^{-1}$  while the Seebeck coefficient was up to  $65 \mu\text{V K}^{-1}$ . Both values of hybrid films were about several times higher than the pure PANI or SWCNT film. Such abnormally simultaneous enhancements of electrical conductivity and Seebeck coefficient were attributed to the highly ordered PANI interface layer on the SWCNT surface. The XRD and Raman analyses revealed the synergetic effect of the chain-expansion by the chemical interactions between PANI and solvent and the chain-ordering aligned by the  $\pi$ - $\pi$  conjugation between PANI and CNT. By contrast, the thermal conductivities still remained at a low level of  $0.43 \text{ W m}^{-1} \text{K}^{-1}$ . Consequently, the best TE power factor and  $zT$  value at room temperature reached  $176 \mu\text{W m}^{-1} \text{K}^{-2}$  and 0.12, respectively.

In addition, by using thick CNT networks as the template, remarkably enhanced Seebeck coefficients and power factors were both obtained in PANI/CNT composites, which are several times larger than either of their individual components.<sup>62</sup> This behavior may be attributed to the size-dependent energy-filtering effect caused by the nanostructured PANI coating layer enwrapped around the CNTs. Relatively low thermal conductivities were also obtained. Moreover, this nanocomposite exhibited great flexibility—can be rolled up, bent, or twisted easily, and even folded without cracking. More recently, a 3D CNT network was used in such PANI-based composites for enhanced TE performance.<sup>63</sup> The 3D CNT network maintains an extremely low thermal conductivity of only  $0.035 \text{ W m}^{-1} \text{K}^{-1}$  in a standard atmosphere at room temperature. Its electrical conductivity could be adjusted through a convenient gas-fuming doping process. By potassium (K) doping, the original p-type CNT network was converted to n-type, whereas iodine ( $\text{I}_2$ ) doping enhanced its electrical conductivity. The self-sustainable homogeneous network structure of the as-fabricated 3D CNT network made it a promising candidate as the template for polymer composition.

Furthermore, multilayered CNTs/polyvinylidene fluoride composites were made into multiple element modules that resemble a felt fabric.<sup>64</sup> The TE voltage generated by these fabrics is the sum of contributions from each layer, resulting in increased power output. Since these fabric-modules have the advantages of low cost, light weight, and simple process over inorganic TE counterparts, the overall performance of the fabric shows good promise as a realistic alternative in numerous applications such as portable electronics.

The CNT/polymer nanocomposites can be also printed on a flexible polyethylene naphthalate film substrate to obtain flexible and lightweight thermoelectric generators (TEGs).<sup>65</sup> The TE composites consisting of CNTs and polystyrene contained approximately 35 vol% of voids, which resulted in remarkably lightweight TEG ( $\sim 15.1 \text{ mg cm}^{-2}$ ). A high power output of approximately  $55 \text{ mW m}^{-2}$  was observed in the TEG at a temperature difference of  $70 \text{ }^\circ\text{C}$ . The TEG maintained no mechanical damage even under bending at a radius of less than 6 mm.

Yu and Grunlan *et al.* have prepared phase-segregated nanocomposites based on the CNT network and polymer, and measured their TE properties as a function of CNT concentration at room temperature (Fig. 10).<sup>66</sup> This study showed that electrical conductivity can be dramatically increased by creating a network of CNTs in the composite, while the thermal conductivity and thermopower remained relatively insensitive to the filler concentration. This behavior was believed to result from thermally disconnected yet electrically connected junctions in the nanotube network, which makes it feasible to tune the properties for higher  $zT$  values. With a CNT concentration of 20 wt%, these composites exhibited an electrical conductivity of  $4800 \text{ S m}^{-1}$ , thermal conductivity of  $0.34 \text{ W m}^{-1} \text{K}^{-1}$  and a  $zT$  value of  $>0.006$  at room temperature.

It was further found that the TE properties of CNT-filled polymer composites can be enhanced by modifying junctions between CNTs using PEDOT:PSS, yielding high electrical

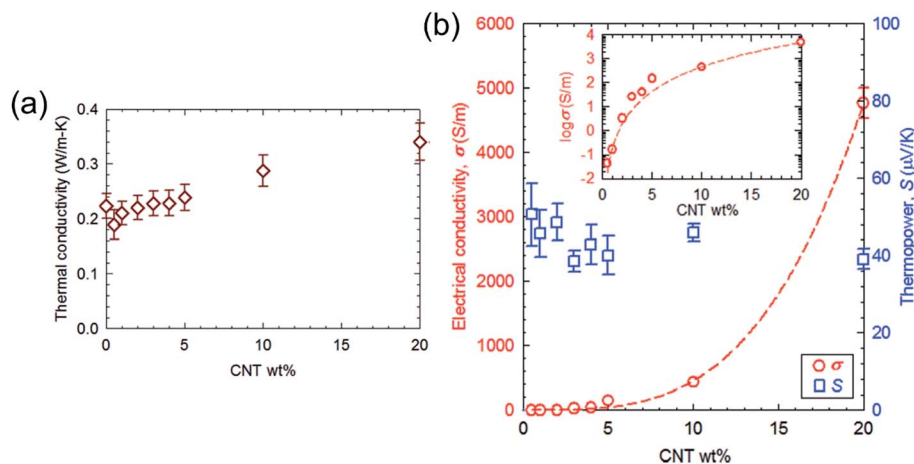


Fig. 10 Thermoelectric performance of CNT-polymer composites at room temperature: (a) thermal conductivity and (b) electrical conductivity (indicated by red circles) and thermopower (indicated by blue squares) as a function of the CNT concentrations (up to 20 wt%). Reprinted with permission from ref. 66. Copyright 2008 The American Chemical Society.

conductivities (up to  $\sim 40\,000\text{ S m}^{-1}$ ) without significantly altering the Seebeck coefficient.<sup>67</sup> This is because PEDOT:PSS particles were decorated on the surface of CNTs and presumably bridged tube-tube junctions, thereby electrically connecting junctions between CNTs. This electrically conducting PEDOT:PSS assisted electrons (*i.e.*, holes) to travel more efficiently in the composites, resulting in high electrical conductivity. On the other hand, thermal transport across the tube-tube junctions remained comparable to typical polymeric materials due to the dissimilar bonding and mismatched vibrational spectra between CNTs and PEDOT:PSS. This behavior was very different from that of typical semiconductors whose TE properties are strongly correlated. The decoupled TE properties, which is ideal for developing better TE materials, are believed to be due to these thermally disconnected and electrically connected contact junctions between CNTs.

The nanocomposites of CNT/PEDOT:PSS (CLEVIOS PH1000 and PH500) were found to exhibit very high electrical conductivities and relatively constant thermopowers which were weakly correlated with electrical conductivities.<sup>68</sup> This resulted in a large power factor of  $\sim 160\ \mu\text{W m}^{-1}\text{ K}^{-2}$  in the in-plane direction of the composites at room temperature, which are orders of magnitude larger than those of typical polymer composites. The optimum nanotube concentrations for better power factors were identified to be 60 wt% in a blend. The highest electrical conductivity and thermopower along the in-plane direction reached  $1.35 \times 10^5\text{ S m}^{-1}$  and  $41\ \mu\text{V K}^{-1}$  at room temperature, respectively. Without additional DMSO doping, PH1000 showed higher thermopowers while PH500 had better electrical conductivities. In contrast, the thermal conductivities of the 60 wt% nanotube composites in the out-of-plane direction were measured to be  $0.2\text{--}0.4\text{ W m}^{-1}\text{ K}^{-1}$  at room temperature. It was however noticed that high nanotube concentrations above 60 wt% decreased the electrical conductivity of the composites due to less effective nanotube dispersions.

The Yu and Grunlan team lately developed both p- and n-type fabric-like flexible light-weight materials by functionalizing

the large surfaces and junctions in CNT mats.<sup>69</sup> Original CNTs, which showed only p-type behaviors with small thermopower values, were successfully converted into both p- and n-type TE materials with large self-powering capability. A TE device based on these CNT films was fabricated, generating enough electrical power to operate a glucose sensor. The electronic transport properties were precisely controlled by changing the amount of coating on CNTs for p-type films as well as treating CNTs with multiple chemical reductants such as polyethylenimine (PEI), diethylenetriamine (DETA), and  $\text{NaBH}_4$  for n-type films. When CNT surfaces are functionalized by molecules or chemical agents, electronic transport across CNT-molecule-CNT junctions can be optimized to increase the thermopower by creating a small energy barrier, while phonon transport are inhibited due to dissimilar vibrational characteristics between CNTs and molecules. Thus, by optimizing the mixing ratio of PEI to DETA at 67 : 33 wt%, n-type thermopower values as large as  $-86\ \mu\text{V K}^{-1}$  at  $5200\text{ S m}^{-1}$  were obtained due to synergistic effects from both large and small dopant molecules. The  $E_F$  values of the p-type samples ( $-4.91\text{ eV}$ ) were changed to  $-4.69\text{ eV}$  after PEI/DETA reduction and  $-4.61\text{ eV}$  after additional  $\text{NaBH}_4$  reduction, *via* Kelvin probe measurements, clearly indicating n-type conversion after the doping processes. The n-type CNT films exhibited a lower electron mobility (*ca.*  $0.206\text{ cm}^2\text{ V}^{-1}\text{ s}^{-1}$ ) than hole mobility (*ca.*  $0.365\text{ cm}^2\text{ V}^{-1}\text{ s}^{-1}$ ), presumably due to the electrically insulating PEI/DETA that impeded the carrier transport across the junctions between CNTs. The high carrier densities of  $1.86 \times 10^{21}\text{ cm}^{-3}$  for p-type and  $1.25 \times 10^{21}\text{ cm}^{-3}$  for n-type, respectively, suggested that it is necessary to further increase the charge mobility for obtaining higher electrical conductivity. The TE device was made of 72 p-type and 72 n-type CNT films electrically connected in series and thermally in parallel in order to maximally utilize temperature gradients. This device produced 465 mV at a temperature gradient of 49 K, far exceeding those of other polymer based composites.

Carbon nanosheets were apparently more effective fillers than CNTs, at comparable loading levels, for producing

polymeric nanocomposites with high thermal conductivity.<sup>70</sup> The thermal conductivity of polymeric nanocomposites is known to be mechanistically limited by the polymer/nanofiller interfacial thermal resistance. Heat transport in polymeric nanocomposites is conducted by phonons of varying frequencies. When reaching the polymer/nanofiller interface, phonons would slow down due to material characteristics such as the largely amorphous nature of the polymer. Nanosheets such as 2D nanofillers could greatly reduce the overall number of polymer/nanofiller interfaces in the resulting polymeric nanocomposites, which in turn leads to ultrahigh thermal conductivities.

Graphene—another important class of carbon materials—has been used with conducting polymers to generate flexible TE modules.<sup>71</sup> PANI/graphene nanocomposite films with three types of graphenes with different structure characteristics were prepared through a solution-assistant dispersing method. It was found that structural defects and oxygen content in the graphene were closely related to the TE performance of the resulting composites. Higher TE properties were obtained in the composite film using graphene with lower levels of structural defects and oxygen impurities. The conformation of PANI molecules was first changed from a compacted coil to an expanded coil by the chemical interactions between PANI and *m*-cresol solvent and then was further expanded by the strong  $\pi$ - $\pi$  stacking between PANI and graphene. The highly expanded molecular conformation of PANI facilitated the chain ordering during solvent evaporation while decreasing the structural defects along the backbone, thus leading to the increase in carrier mobility. Ultimately, the maximum electrical conductivity and power factor of the composite films reached  $856 \text{ S cm}^{-1}$  and  $19 \mu\text{W m}^{-1} \text{ K}^{-2}$ , respectively.

### 3.2 Polymer/inorganic nanocrystal hybrids

Another effective approach to enhance the TE properties is to incorporate high-TE performance inorganic TE components such as  $\text{Sb}_2\text{Te}_3$  and  $\text{Bi}_2\text{Te}_3$  in the nanocomposites.<sup>19,20</sup> These nanocomposites are expected to exhibit better TE performance than the neat polymer due to the synergistic effects from combined advantages of the polymer and nanocrystal. Generally, such polymer–inorganic nanostructure based hybrid films are easily made by solution processing methods such as spin-coating, drop-casting, and spraying. Selection of suitable polymer matrices and inorganic TE nanostructures can be accomplished *via* computational modelling such that the interplay and volume fraction of each phase is optimized to maximize the  $zT$  value of the composite. However, how to rationally engineer the polymer–inorganic interface to improve the TE performance remains a challenging task. Some of the concepts in inorganic nanostructures such as phonon scattering, carrier-energy-filtering, and carrier-pocket engineering may also be adopted in polymer TE materials, which yet needs several important principles for constructing energy filtering interfaces in polymer–inorganic nanocomposites.

The TE composites of hexagonal shaped p-type  $\text{Sb}_2\text{Te}_3$ /PEDOT were fabricated by embedding PEDOT into a  $\text{Sb}_2\text{Te}_3$

matrix.<sup>72</sup> The thermal conductivity of the composites was significantly reduced down to  $0.148 \text{ W m}^{-1} \text{ K}^{-1}$  from  $0.398 \text{ W m}^{-1} \text{ K}^{-1}$  of pure  $\text{Sb}_2\text{Te}_3$  compounds in the temperature range of 300–523 K, owing to strong scattering of heat carrying phonons by plate-like  $\text{Sb}_2\text{Te}_3$  nanoparticles and the embedded PEDOT. The composites displayed good thermal stability and remained low  $\kappa$  even after 50 periodic thermal cycles in the temperature range from room temperature to 523 K. The electrical conductivity of the composites was not subject to a significant change while  $S$  increased. The  $zT$  value of the composites reached 1.18 at 523 K, increased by 60% compared with that of the pure  $\text{Sb}_2\text{Te}_3$  sample. In another example, by incorporating both n and p-type  $\text{Bi}_2\text{Te}_3$  ball milled powders into PEDOT:PSS (CLEVIOS PH1000), power factors were enhanced.<sup>73</sup> Yet, the contact resistance between  $\text{Bi}_2\text{Te}_3$  and PEDOT was identified as the limiting factor for further TE property improvement.

A facile route was made to PEDOT and PbTe-modified PEDOT nanotubes for TE applications.<sup>74</sup> The nanotubes were prepared by an *in situ* interfacial polymerization method by adding PbTe nanoparticles into a polymerization medium. The pure de-doped PEDOT exhibited n-type conduction and had an extremely large Seebeck coefficient of  $-4088 \mu\text{V K}^{-1}$  yet a low electrical conductivity of  $0.064 \text{ S m}^{-1}$ . The electrical conductivity of the composite powders after cold pressing increased with an increasing PbTe content, and the power factor could be tuned by adjusting the PbTe content accordingly.

Water-soluble composites composed of a tellurium (Te) nanocrystal core functionalized with PEDOT:PSS were prepared for TE applications.<sup>75</sup> Such PEDOT:PSS functionalized Te nanocrystal films electronically outperformed either PEDOT:PSS or unfunctionalized Te nanorods while retaining a polymeric thermal conductivity, resulting in a room temperature  $zT$  value of  $\sim 0.1$ . This combination of electronic and thermal transport holds great potential for tailored transport in nanoscale organic/inorganic heterostructures.

Yet, unusual electrical transport behavior was observed in high-performance TE composites of PEDOT:PSS/Te nanowires.<sup>76</sup> With increasing Te contents in the hybrid films, the electrical conductivity exhibited a peak while the Seebeck coefficient increased. This was accurately described by a series-connected model where carrier transport occurs predominantly through a highly conductive volume of the polymer that exists at the nanowire/polymer interface. The results stressed the importance of understanding and controlling interfacial phenomena in hybrid organic–inorganic systems, and provided a general route for enhancing carrier transport in hybrid materials and devices.

Later, microribbons of the Te nanowire/PEDOT:PSS composite were fabricated by a standard lift-off process.<sup>77</sup> Positive temperature dependent electrical conductivity and Seebeck coefficient of the composite were found in the temperature range of 10–400 K, revealing a complex, thermally activated mechanism. In addition, aging of the TE device was investigated. With the oxidation of the Te nanowires, the resulting composites showed a slight decrease in electrical conductivity and doubled Seebeck coefficient at room temperature.

## 4. When thermoelectrics meet photovoltaics—photothermalelectrics

There are two main paths to utilize solar energy, that is, photovoltaic and thermoelectric techniques. These two paths are however limited on their own. (1) For photovoltaics, the transfer of energy from photons to electrons highly relies on the band gap of the working materials. With a higher band gap, fewer photons could be absorbed and the quantum efficiency would be lowered; on the other hand, with a lower band gap which guarantees high quantum efficiency, the voltage output capability could be lowered since the energy of the excited state is too low, leading to energy loss in the photon energy transfer. As a result, the utilization of photon energy is largely limited. (2) For thermoelectrics, the energy of photons in the sunlight is transferred to heat in the first place, which inevitably leads to energy loss. Arguably, combination of these two complementary energy conversion methods would benefit each other and represent a powerful way to harvest the sun energy more efficiently. For example, in two most recent reports, researchers have demonstrated the integration of an organic solar cell with a commercial thermoelectric module to improve the electric energy output capability.

Kim *et al.* reported the first near-infrared (NIR) active conjugated polymer that has photothermal (PT) effect and TE properties simultaneously.<sup>78</sup> Both PT conversion and TE effect can successfully convert the light-driven heat into electricity, making photo-thermo-electric (PTE) conversion possible in a single device. In their work, the poly(3,4-ethylenedioxyphenylene) (PEDOS-C6) film which displayed a visible to NIR electrochromic (EC) effect was examined for the PTE process. Fig. 11 shows the doping control process of the PEDOS-C6 film and the fabrication steps of the PTE harvester.

PEDOS-C6 films prepared by the constant potential method (namely, CPP) can be easily investigated according to the film thickness and absorption intensity, without invoking the roughness effect. The CPP films were strongly colored in the NIR inactive state (dedoped state), while bleached in the NIR active state (doped state). This evident visible to/from NIR electrochromism led to the effective control in the doping process of the film. As a consequence, the PT conversion efficiency can be greatly increased from 16.1 to 42.5% while minimizing the visible light absorption in a doped film at  $-0.1$  V. Besides, this film exhibited the highest TE effect with a maximum power factor of  $354.7 \mu\text{W m}^{-1} \text{K}^{-2}$  at  $-0.1$  V. Furthermore, the work demonstrated a flexible film device with such combined EC, PT and TE properties, which could be also used for invisible NIR sensors and multifunctional film displays.

In another study, researchers in China demonstrated a high-performance polymer solar cell–thermoelectric (PSC–TE) hybrid energy-harvesting system, which realized harvesting of electricity from solar light and solar heat simultaneously.<sup>79</sup> In the PSC–TE devices, a TE module consisting of  $\text{Bi}_2\text{Te}_3$  based compounds was attached to the backside of a PSC device based on the blend of P3HT and a new indene- $\text{C}_{60}$  bisadduct ( $\text{IC}_{60}\text{BA}$ ). In this hybrid system, the PSC acted as the “top cell” and the TE module served as the “bottom cell”. PSC and TE were connected in series and worked as two power supplies. With the PSC utilizing visible light and the TE module exploiting the remaining parts of the solar energy as well as converting heat to electricity, the open-circuit voltage and the power output were improved dramatically. When a temperature gradient was introduced across the TE module, the output power of the PSC–TE system was improved by 46.6% as compared to the performance of a single PSC, giving the best output power up to  $11.29 \text{ mW cm}^{-2}$ . Interestingly, the hybrid system can drive a

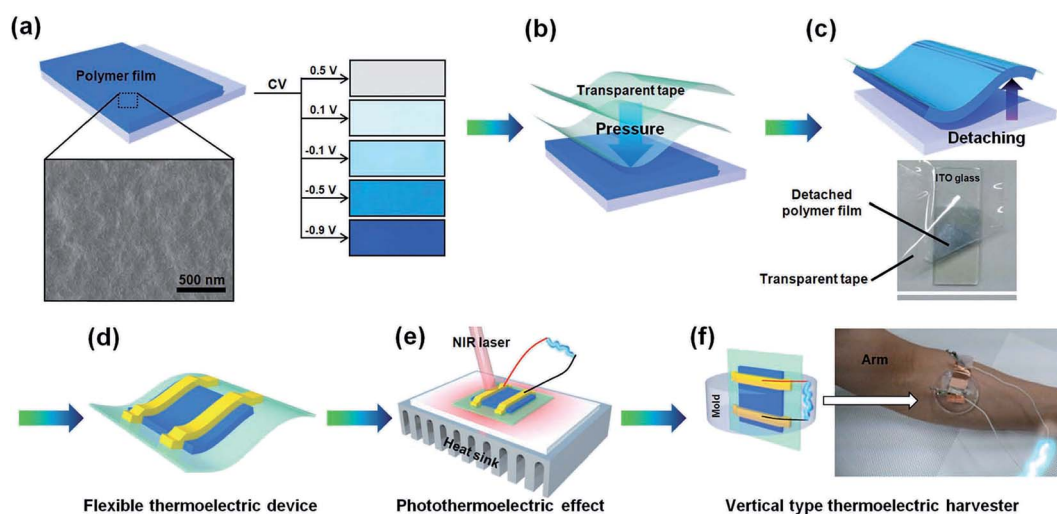


**Fig. 11** The doping control of the PEDOS-C6 film and the fabrication of the PTE harvester. (a) The photo images of doping controlled PEDOS-C6 films on ITO glass. A SEM image of the pristine CPP film. (b and c) Detaching process from the ITO glass to transparent tape. A photo image shows the film clearly detached from the ITO glass. (d) Flexible TE device with Au electrode deposition in the vacuum chamber. (e) The measurement setting of the PTE effect and (f) the vertical type TE harvester on an arm for generating thermoelectricity from body heat. Reprinted with permission from ref. 78. Copyright 2013 Wiley-VCH.

commercial light-emitting diode by effectively utilizing solar energy over a broad wavelength range, which however cannot be realized by either PV or TE device alone. Overall, such a hybrid system has proved to be a promising configuration towards obtaining the electricity by integrating multiple devices with different functions, and better performance is expected by optimum materials design and device structures.

## 5. Challenges of organic TE materials

### 5.1 Stability

Despite encouraging TE performances, the thermal stability of organic semiconductors remains a major issue for practical TE applications. Most organic semiconductors can only sustain the temperature below 300 °C, while inorganic materials can be stable over a broad range of temperatures up to 1000 °C. As a result, organic TE materials will compete with their inorganic counterparts mainly in cooling systems and low-temperature power generators, favorably in flexible modules. In this regard, organic TE materials are more likely to extend the TE applications rather than replacing the inorganic counterparts.

Studies have shown that the stability of low temperature of organic TE materials is promising. For instance, it was reported that PEDOT:PSS films could be heated in air at 100 °C for over 1000 h with only a minimal change in conductivity.<sup>80</sup> Additionally, de-doped PEDOT-Tos was stable at temperatures from room temperature up to 100 °C in air.<sup>41</sup> Both examples have opened up possibilities of practical applications for organic TE materials.

Strategies such as increasing molecular weight and regularity would help improve the thermal stability of organic TE materials. In this respect, chemistry plays an important role by rational design of appropriate molecular structures such as introducing rigid groups in the backbone or side chains. For instance, the stability of 2,7-carbazole-based polymers was highly improved by replacing the vinylene unit by electron-donating conjugated units such as thiophene or bis(3,4-ethylenedioxythiophene).<sup>17</sup>

Ambient stability is another concern for organic TE materials due to the sensitivity of organic semiconductors to moisture

and oxygen. Appropriate encapsulation of the organic films to block the adsorption of molecular oxygen and water vapor will be necessary for practical thermal energy harvesting applications. Fortunately, vast experiences of encapsulation used in organic electronic devices—especially flexible encapsulation technology—could largely aid the development for practical organic TE applications. Specifically, there existed several strategies for encapsulation of organic light-emitting diodes and photovoltaic cells, including multi-layered barriers formed *via* plasma enhanced chemical vapor deposition and atomic layer deposition, and polymer (*e.g.*, poly(dimethylsiloxane), PDMS) thin film encapsulation.<sup>81</sup> In addition, encapsulation of flexible organic devices can be done by the lamination process utilizing optically clear adhesive in the form of gasket.<sup>82</sup> The use of the transparent adhesive as gasket could simplify the encapsulation process while securing the gas barrier properties in the sealing section.

### 5.2 Sample preparation and measurement techniques

Sample preparation is crucial for accurate measurements. The traditional methods of preparing inorganic TE materials include ball milling and hot pressing, which are yet unsuitable for solution-processed organic TE materials. Organic TE materials are usually in the film form made by spin-coating and drop-casting. In particular, *in situ* oxidative/interfacial polymerization/intercalation were employed to fabricate organic/inorganic TE nanocomposites.<sup>19</sup>

Owing to the anisotropic behavior of organic TE films caused by solution processing, characterization of TE properties becomes sophisticated with various resulting problems. Yet, some measurement techniques have recently appeared as displayed in Table 2, holding good promise for reliable characterization of organic TE materials. Still, more are awaiting.

Special care should be paid to the TE measurements. For electrical measurements, the resistance of the organic TE samples must be several orders of magnitude smaller than that of the substrates; otherwise, the current would go through the substrates other than the samples. Often, the electrical conductivity is measured by two-contact or four-contact

Table 2 Summarized methods in the literature for characterizing the thermoelectric properties of organic thermoelectric materials

| Parameters | Measurements   |
|------------|--|
| $\sigma$   | (1) Four-contact measurement <sup>62,67–69</sup><br>(2) Two-contact method <sup>8</sup>  |
| $\rho_f$   | (1) Hall measurement <sup>10–12</sup><br>(2) Capacitance–voltage analysis <sup>83,84</sup>   |
| $\kappa$   | $\kappa_{\text{in-plane}}$<br>(1) Steady-state measurement (100 $\mu\text{m}$ ) <sup>8</sup><br>(2) Three-omega ( $3\omega$ ) method <sup>8</sup>  |
|            | $\kappa_{\text{out-of-plane}}$<br>(1) Transient-state measurement: (a) ultrafast pump–probe laser flash technique <sup>70,72</sup> and (b) time domain thermal reflectance (TDTR) <sup>51</sup><br>(2) Steady-state method (ASTM D5470) <sup>67,68</sup><br>(3) Three-omega ( $3\omega$ ) method <sup>8</sup><br>(4) TCI thermal conductivity analyzer (C-Therm Tech.) <sup>51</sup> |
| $S$        | (1) ZEM-3 system (ULVAC Tech.) <sup>72</sup><br>(2) SB-100 system (MMR Tech.) <sup>8</sup>   |

measurement. The four-probe method is more preferred due to elimination of the contributions of the current leads or the contacts in the sample voltage measurement.<sup>9</sup> The doping level or carrier concentration in organic semiconductors can be characterized by the Hall measurement<sup>10–12</sup> or favorably by capacitance–voltage analysis.<sup>83,84</sup> But for the measurements of Seebeck coefficient and thermal conductivity, self-supporting films are usually required, which can be achieved by removal of the substrates using bulk or surface micromachining (*e.g.*, by a sacrificial layer technology or by selective plasma dry etching).<sup>9</sup> For instance, a free-standing PEDOT:PSS film can be obtained by the following method.<sup>49</sup> A 1 mm thick cross-linked PDMS film was prepared in a 20 mL polystyrene bottle. Subsequently, PEDOT:PSS solution was added and the polystyrene bottle was heated on a hot plate at 70 °C. After removing all the solvents, the PEDOT:PSS film was easily detached from the PDMS substrate. The free-supporting film was then cut into required rectangular shapes for measurement. In short, reliable TE measurement techniques—preferably home-made apparatuses with customized controls—are highly needed to be developed for organic thin films on substrates.

## 6. Conclusions and perspectives

To conclude, we have reviewed recent advances (update to September 2014) in organic TE materials, in which tremendous work has been conducted to offer various strategies of improving the TE performances. Yet some critical issues in TEs need to be resolved before their well-developments into the stage where organic (opto)electronics are. The most challenging issue is the lack of straight yet reliable characterization methods owing to the state of thin film and anisotropy of organic TE materials. Encouragingly, some measurement techniques have recently appeared as shown in Table 2, yet more are awaiting. Moreover, an effective combination of experimental and simulation work is expected to be capable of suggesting feasible strategies for maximal optimization of organic TE performances. A key to this end is to clarify both electrical and thermal transport mechanisms of organic semiconductors in TE applications. In this regard, theoretical models will aid the design of suitable organic-based nanocomposites and properly engineered interfaces, thus optimizing the TE performance. Experimentally, it is important to enhance the crystallinity, control the structure and surface morphology of organic materials, and optimize the doping level, thereby collectively leading to the balanced TE properties while simultaneously engineering an electronic structure that provides favorable DoS and  $E_F$ .

Arguably, the optimization of TE performance for organic materials is just in its infancy. Various methods of doping treatments have been adopted to balance the  $\sigma$  and  $S$  for a maximum power factor ( $S^2\sigma$ ). However, excessive doping would generate detrimental defects and traps, which reduces  $\mu$  and limits  $S$ . A reasonable way of TE optimization is to obtain highly intrinsic  $\mu$  by careful design of suitable molecular structures of organic semiconductors—planar and regioregular structures favor molecular packing and facilitate charge transport. Meanwhile, an optimal low doping level is maintained, yielding a comparatively

low  $p_F$ . As a result, smaller  $\sigma$  is obtained according to eqn (2.1). However, reduced  $\sigma$  can be compensated by significantly improved  $S$  due to the low level of doping, collectively giving rise to the maximum power factor. On the other side, the thermal conductivity in organic TE materials is generally recognized to be dominated by  $\kappa_L$ . Thus another parallel way of TE optimization would be constructing (quasi-)one-dimensional organic nanostructures which confine thermal vibrations while benefiting the carrier mobility owing to anisotropic charge transport, or fabricating organic–inorganic nanocomposites where the presence of grain boundaries and rich interfacial interfaces significantly scatter phonons. Both approaches largely decrease  $\kappa_L$ . Together, it can be seen that TE property parameters are able to be decoupled in organic TE materials, in stark contrast to those of conventional inorganic analogues, therefore showing great promise of organic TEs. Still, the pursuit of new organic materials with more desirable TE properties should move forward. Most recently, the first-principles studies of hybrid perovskites— $\text{CH}_3\text{NH}_3\text{Al}_3$  ( $A = \text{Pb}$  and  $\text{Sn}$ ), which have recently captured great successes in photovoltaic applications, have suggested that these systems may be excellent materials for solar TE applications.<sup>85</sup> Theoretical predictions showed that these perovskites might exhibit (i) large values of intrinsic  $\mu$  due to small carrier effective masses and weak electron–phonon and hole–phonon couplings, and (ii) large values of  $S$  owing to the multiply degenerate conduction and valence bands. The  $zT$  values of these perovskites could reach 1 to 2, given  $p_F$  on the order of  $\sim 10^{18} \text{ cm}^{-3}$ .

Ultimately, what makes organic TE materials stand out is the solution processing of flexible TE modules, which is indeed difficult to realize in inorganic TE materials. Owing to the advantages of cost-effectiveness, light-weight, and scalable production methods, organic TE materials hold great promise in a range of applications such as flexed or curved TE module devices and wearable electronic devices operated by body heat. Additionally, a vast amount of valuable experiences in flexible organic electronic devices could be utilized for the development of flexible TE modules. Interestingly, cuttable, durable and transparent TE electronic devices could be achieved through customized organic materials (*e.g.*, PEDOT:PSS). More importantly, manufacturing methods such as screen-printing, ink-jet printing and roll-to-roll printing have been shown to be scalable methods for production of organic TE generators. With all these exciting advances in organic TE materials, the development of personal, portable, and flexible thermal modules will no longer be just a possibility.

## Abbreviations

| Abbreviation | Full name  | References |
|--------------|--|------------|
| $z$          | Figure of merit  |            |
| $T$          | Temperature (K)  |            |
| $S$          | Seebeck coefficient ( $\text{V K}^{-1}$ )                |            |
| $\sigma$     | Electrical conductivity ( $\text{S m}^{-1}$ )            |            |
| $\kappa$     | Thermal conductivity ( $\text{W m}^{-1} \text{K}^{-1}$ ) |            |
| $\kappa_L$   |  |            |

(Contd.)

| Abbreviation        | Full name  | References |
|---------------------|--|------------|
|                     | Phonon contribution to thermal conductivity ( $\text{W m}^{-1} \text{K}^{-1}$ )  |            |
| $\kappa_e$          | Electron contribution to thermal conductivity ( $\text{W m}^{-1} \text{K}^{-1}$ )  |            |
| $\eta$              | Conversion efficiency  |            |
| $p_f$               | Free carrier density ( $\text{cm}^{-3}$ )  |            |
| $\mu$               | Charge carrier mobility ( $\text{cm}^2 \text{V}^{-1} \text{s}^{-1}$ )  |            |
| $q$                 | Electronic charge ( $1.6 \times 10^{-19} \text{C}$ )   |            |
| $E_F$               | Fermi level  |            |
| DoS                 | Density of state   |            |
| TEG                 | Thermoelectric generator   |            |
| PEDOT               | Poly(3,4-ethylenedioxythiophene)   | 9          |
| $E_T$               | Conduction band  | 9          |
| CSA                 | Camphor sulfonic acid  | 25         |
| PCDTBT              | Poly[ <i>N</i> -(7'-heptadecanyl-2,7-carbazole- <i>alt</i> -5,5'-(4',7'-di-2-thienyl-2',1',3'-benzothiadiazole)]                                       | 29         |
| PANI                | Polyaniline  | 29         |
| P3HT                | Poly(3-hexylthiophene)   | 30         |
| P3HTT               | Poly(3-hexylthiothiophene)   | 30         |
| F <sub>4</sub> TCNQ | 2,3,5,6-Tetrafluoro-7,7,8,8-tetracyanoquinodimethane   | 30         |
| TTF                 | Tetrathiafulvalene   | 31         |
| P(NDIOD-T2)         | Poly[ <i>N,N'</i> -bis(2-octyl-dodecyl)-1,4,5,8-naphthalenedicarboximide-2,6-diyl]- <i>alt</i> -5,5'-(2,2'-bithiophene)]                               | 32         |
| <i>N</i> -DMBI      | Dihydro-1 <i>H</i> -benzimidazol-2-yl  | 32         |
| <i>N</i> -DPBI      | 4-(1,3-Dimethyl-2,3-dihydro-1 <i>H</i> -benzimidazol-2-yl)- <i>N,N</i> -diphenylaniline  | 32         |
| PDI                 | Perylene diimide   | 34         |
| CPEs                | Conjugated polyelectrolytes  | 35         |
| TBA                 | Tetrabutylammonium   | 35         |
| PSBTBT              | Poly[(4,4'-bis(2-ethylhexyl)dithieno[3,2- <i>b</i> :2',3'- <i>d</i> ]silole)-2,6-diyl- <i>alt</i> -(2,1,3-benzothiadiazole)-4,7-diyl]                  | 36         |
| PDPP3T              | Poly[{2,5-bis(2-hexyldecyl)-2,3,5,6-tetrahydro-3,6-dioxopyrrolo[3,4- <i>c</i> ]pyrrole-1,4-diyl]- <i>alt</i> -{[2,2':5',2''-terthiophene]-5,5''-diyl}] | 36         |
| PBTTT               | Poly(2,5-bis(3-dodecylthiophen-2-yl)thieno[3,2- <i>b</i> ]thiophene)   | 36         |
| IPN                 | Interpenetrating networks  | 38         |
| P3BT                | Poly(3-butylthiophene)   | 38         |
| BTFMSI              | Bis(trifluoromethylsulfonyl)imide  | 39         |
| PEPG                | Poly(ethylene glycol)- <i>block</i> -poly(propylene glycol)- <i>b</i> -poly(ethylene glycol) tri-block copolymer                                       | 40         |
| EDOT                | 3,4-Ethylenedioxythiophene   | 40         |
| Tos                 | Tosylate   | 40         |
| TDAE                | Tetrakis(dimethylamino)ethylene  | 41         |
| CB                  | Conduction band  | 43         |
| VB                  | Valance band   | 43         |
| DMSO                | Dimethyl sulfoxide   | 46         |
| HZ                  | Hydrazine  | 46         |
| EG                  | Ethylene glycol  | 47         |
| PTh                 | Polythiophene  | 48         |
| BFEE                | Boron trifluoride diethyl ether  | 48         |
| P3MeT               | Poly(3-methylthiophene)  | 48         |
| PBO                 | Polybenzobisoxazole  | 51         |
| PE                  | Polyethylene   | 42         |
| HOMO                | Highest occupied molecular orbital   | 53         |
| LUMO                | Lowest unoccupied molecular orbital  | 53         |
| BDT                 | Benzenedithiol   | 53         |
| DBDT                | 4,4'-Dibenzenedithiol  | 53         |
| TBDT                | 4,4''-Tribenzenedithiol  | 53         |

(Contd.)

| Abbreviation | Full name   | References |
|--------------|---|------------|
| PCBM         | [6,6]-Phenyl-C61-butyric acid methyl ester                        | 54         |
| MEH-PPV      | Poly(2-methoxy-5-(2'-ethylhexyloxy)- <i>p</i> -phenylene vinylene | 59         |
| SWCNT        | Single-walled carbon nanotube                                     | 60         |
| MWCNT        | Multi-walled carbon nanotube                                      | 60         |
| CNT          | Carbon nanotube   | 60         |
| PEI          | Polyethylenimine  | 69         |
| DETA         | Diethylenetriamine  | 69         |
| NIR          | Near-infrared   | 78         |
| PT           | Photothermal  | 78         |
| EC           | Electrochromic  | 78         |
| PTE          | Photo-thermo-electric   | 78         |
| CPP          | Constant potential method   | 78         |
| PEDOS-C6     | Poly(3,4-ethylenedioxysephenophene)                               | 78         |
| PSC-TE       | Polymer solar cell-thermoelectric                                 | 79         |

## Acknowledgements

We are grateful to the reviewers for their valuable comments and insightful suggestions. Our work on organic thermoelectrics is sponsored by Shanghai Pujiang Program (2013), no. 13PJ1400500.

## References

- 1 M. Zebarjadi, K. Esfarjani, M. S. Dresselhaus, Z. F. Ren and G. Chen, *Energy Environ. Sci.*, 2012, **5**, 5147–5162.
- 2 S. K. Yee, S. LeBlanc, K. E. Goodson and C. Dames, *Energy Environ. Sci.*, 2013, **6**, 2561–2571.
- 3 L.-D. Zhao, V. P. Dravid and M. G. Kanatzidis, *Energy Environ. Sci.*, 2014, **7**, 251–268.
- 4 Y. Zhang and G. D. Stucky, *Chem. Mater.*, 2014, **26**, 837–848.
- 5 Y. Pei, H. Wang and G. J. Snyder, *Adv. Mater.*, 2012, **24**, 6125–6135.
- 6 J. P. Heremans, B. Wiendlocha and A. M. Chamoire, *Energy Environ. Sci.*, 2012, **5**, 5510–5530.
- 7 C. Xiao, Z. Li, K. Li, P. Huang and Y. Xie, *Acc. Chem. Res.*, 2014, **47**, 1287–1295.
- 8 G. Dennler, R. Chmielowski, S. Jacob, F. Capet, P. Roussel, S. Zastrow, K. Nielsch, I. Opahle and G. K. H. Madsen, *Adv. Energy Mater.*, 2014, **4**, 1301581.
- 9 D. M. Rowe, *Thermoelectrics Handbook: Macro to Nano*, CRC Press, 2005.
- 10 K. Biswas, J. He, Q. Zhang, G. Wang, C. Uher, V. P. Dravid and M. G. Kanatzidis, *Nat. Chem.*, 2011, **3**, 160–166.
- 11 K. Biswas, J. He, I. D. Blum, C.-I. Wu, T. P. Hogan, D. N. Seidman, V. P. Dravid and M. G. Kanatzidis, *Nature*, 2012, **489**, 414–418.
- 12 S. N. Guin, A. Chatterjee, D. S. Negi, R. Dattab and K. Biswas, *Energy Environ. Sci.*, 2013, **6**, 2603–2608.
- 13 Y. Pei, Z. M. Gibbs, B. Balke, W. G. Zeier and G. J. Snyder, *Adv. Energy Mater.*, 2014, **4**, 1400486.
- 14 L. Hu, T. Zhu, X. Liu and X. Zhao, *Adv. Funct. Mater.*, 2014, **24**, 5211–5218.

- 15 H. Yang, J.-H. Bahk, T. Day, A. M. S. Mohammed, B. Min, G. J. Snyder, A. Shakouri and Y. Wu, *Nano Lett.*, 2014, **14**, 5398–5404.
- 16 L.-D. Zhao, S.-H. Lo, Y. Zhang, H. Sun, G. Tan, C. Uher, C. Wolverton, V. P. Dravid and M. G. Kanatzidis, *Nature*, 2014, **508**, 373–377.
- 17 N. Dubey and M. Leclerc, *J. Polym. Sci., Part B: Polym. Phys.*, 2011, **49**, 467–475.
- 18 T. O. Poehler and H. E. Katz, *Energy Environ. Sci.*, 2012, **5**, 8110–8115.
- 19 Y. Du, S. Z. Shen, K. Cai and P. S. Casey, *Prog. Polym. Sci.*, 2012, **37**, 820–841.
- 20 M. He, F. Qiu and Z. Lin, *Energy Environ. Sci.*, 2013, **6**, 1352–1361.
- 21 O. Bubnova and X. Crispin, *Energy Environ. Sci.*, 2012, **5**, 9345–9362.
- 22 J. Yang, H.-L. Yip and A. K.-Y. Jen, *Adv. Energy Mater.*, 2013, **3**, 549–565.
- 23 Q. Zhang, Y. Sun, W. Xu and D. Zhu, *Adv. Mater.*, 2014, **26**, 6829–6851.
- 24 Y. Wang, J. Zhou and R. Yang, *J. Phys. Chem. C*, 2011, **115**, 24418–24428.
- 25 D. K. C. MacDonald, *Thermoelectricity: an Introduction to the Principles*, Dover Publications, 2006.
- 26 N. G. Semaltianos, C. Koidis, C. Pitsalidis, P. Karagiannidis, S. Logothetidis, W. Perrie, D. Liu, S. P. Edwardson, E. Fearon, R. J. Potter, G. Dearden and K. G. Watkins, *Synth. Met.*, 2011, **161**, 431–439.
- 27 R. Cagnolati, D. Fioretto, G. Ruggeri and G. Socino, *Synth. Met.*, 1993, **60**, 255–258.
- 28 X. Gao, K. Uehara, D. D. Klug, S. Patchkovskii, J. S. Tse and T. M. Tritt, *Phys. Rev. B: Condens. Matter Mater. Phys.*, 2005, **72**, 125202.
- 29 R. B. Aïch, N. Blouin, A. Bouchard and M. Leclerc, *Chem. Mater.*, 2009, **21**, 751–757.
- 30 J. Sun, M.-L. Yeh, B. J. Jung, B. Zhang, J. Feser, A. Majumdar and H. E. Katz, *Macromolecules*, 2010, **43**, 2897–2903.
- 31 J. Sinha, S. J. Lee, H. Kong, T. W. Swift and H. E. Katz, *Macromolecules*, 2013, **46**, 708–717.
- 32 R. A. Schlitz, F. G. Brunetti, A. M. Glaudell, P. L. Miller, M. A. Brady, C. J. Takacs, C. J. Hawker and M. L. Chabinyc, *Adv. Mater.*, 2014, **26**, 2825–2830.
- 33 Y. Sun, P. Sheng, C. Di, F. Jiao, W. Xu, D. Qiu and D. Zhu, *Adv. Mater.*, 2012, **24**, 932–937.
- 34 B. Russ, M. J. Robb, F. G. Brunetti, P. L. Miller, E. E. Perry, S. N. Patel, V. Ho, W. B. Chang, J. J. Urban, M. L. Chabinyc, C. J. Hawker and R. A. Segalman, *Adv. Mater.*, 2014, **26**, 3473–3477.
- 35 C.-K. Mai, R. A. Schlitz, G. M. Su, D. Spitzer, X. Wang, S. L. Fronk, D. G. Cahill, M. L. Chabinyc and G. C. Bazan, *J. Am. Chem. Soc.*, 2014, **136**, 13478–13481.
- 36 Q. Zhang, Y. Sun, W. Xu and D. Zhu, *Macromolecules*, 2014, **47**, 609–615.
- 37 W. Shi, J. Chen, J. Xi, D. Wang and Z. Shuai, *Chem. Mater.*, 2014, **26**, 2669–2677.
- 38 G. Lu, L. Bu, S. Li and X. Yang, *Adv. Mater.*, 2014, **26**, 2359–2364.
- 39 M. Culebras, C. M. Gómez and A. Cantarero, *J. Mater. Chem. A*, 2014, **2**, 10109–10115.
- 40 T. Park, C. Park, B. Kim, H. Shin and E. Kim, *Energy Environ. Sci.*, 2013, **6**, 788–792.
- 41 O. Bubnova, Z. U. Khan, A. Malti, S. Braun, M. Fahlman, M. Berggren and X. Crispin, *Nat. Mater.*, 2011, **10**, 429–433.
- 42 M. Leclerc and A. Najari, *Nat. Mater.*, 2011, **10**, 409–410.
- 43 O. Bubnova, M. Berggren and X. Crispin, *J. Am. Chem. Soc.*, 2012, **134**, 16456–16459.
- 44 O. Bubnova, Z. U. Khan, H. Wang, S. Braun, D. Evans, M. Fabretto, P. Hojati-Talemi, D. Dagnelund, J.-B. Arlin, Y. H. Geerts, S. Desbief, D. Breiby, J. Andreasen, R. Lazzaroni, W. M. Chen, I. Zozoulenko, M. Fahlman, P. J. Murphy, M. Berggren and X. Crispin, *Nat. Mater.*, 2014, **13**, 190–194.
- 45 M. Chabinyc, *Nat. Mater.*, 2014, **13**, 119–121.
- 46 H. Park, S. H. Lee, F. S. Kim, H. H. Choi, I. W. Cheong and J. H. Kim, *J. Mater. Chem. A*, 2014, **2**, 6532–6539.
- 47 G.-H. Kim, L. Shao, K. Zhang and K. P. Pipe, *Nat. Mater.*, 2013, **12**, 719–723.
- 48 H. Shi, C. Liu, J. Xu, H. Song, B. Lu, F. Jiang, W. Zhou, G. Zhang and Q. Jiang, *ACS Appl. Mater. Interfaces*, 2013, **5**, 12811–12819.
- 49 Q. Wei, M. Mukaida, K. Kirihara and T. Ishida, *ACS Macro Lett.*, 2014, **3**, 948–952.
- 50 D. K. Taggart, Y. Yang, S.-C. Kung, T. M. McIntire and R. M. Penner, *Nano Lett.*, 2011, **11**, 125–131.
- 51 X. Wang, V. Ho, R. A. Segalman and D. G. Cahill, *Macromolecules*, 2013, **46**, 4937–4943.
- 52 S. Shen, A. Henry, J. Tong, R. Zheng and G. Chen, *Nat. Nanotechnol.*, 2010, **5**, 251–255.
- 53 P. Reddy, S.-Y. Jang, R. A. Segalman and A. Majumdar, *Science*, 2007, **315**, 1568–1571.
- 54 S. K. Yee, J. A. Malen, A. Majumdar and R. A. Segalman, *Nano Lett.*, 2011, **11**, 4089–4094.
- 55 S. K. Lee, T. Ohto, R. Yamada and H. Tada, *Nano Lett.*, 2014, **14**, 5276–5280.
- 56 Y. Wang, J. Liu, J. Zhou and R. Yang, *J. Phys. Chem. C*, 2013, **117**, 24716–24725.
- 57 L. Yan, M. Shao, H. Wang, D. Dudis, A. Urbas and B. Hu, *Adv. Mater.*, 2011, **23**, 4120–4124.
- 58 M. Stanford, H. Wang, I. Ivanov and B. Hu, *Appl. Phys. Lett.*, 2012, **101**, 173304.
- 59 L. Xu, Y. Liu, M. P. Garrett, B. Chen and B. Hu, *J. Phys. Chem. C*, 2013, **117**, 10264–10269.
- 60 C. Bounioux, P. Díaz-Chao, M. Campoy-Quiles, M. S. Martín-González, A. R. Goni, R. Yerushalmi-Rozene and C. Müller, *Energy Environ. Sci.*, 2013, **6**, 918–925.
- 61 Q. Yao, Q. Wang, L. Wang and L. Chen, *Energy Environ. Sci.*, 2014, **7**, 3801–3807.
- 62 C. Meng, C. Liu and S. Fan, *Adv. Mater.*, 2010, **22**, 535–539.
- 63 J. Chen, X. Gui, Z. Wang, Z. Li, R. Xiang, K. Wang, D. Wu, X. Xia, Y. Zhou, Q. Wang, Z. Tang and L. Chen, *ACS Appl. Mater. Interfaces*, 2012, **4**, 81–86.
- 64 C. A. Hewitt, A. B. Kaiser, S. Roth, M. Craps, R. Czerw and D. L. Carroll, *Nano Lett.*, 2012, **12**, 1307–1310.

- 65 K. Suemori, S. Hoshino and T. Kamata, *Appl. Phys. Lett.*, 2013, **103**, 153902.
- 66 C. Yu, Y. S. Kim, D. Kim and J. C. Grunlan, *Nano Lett.*, 2008, **8**, 4428–4432.
- 67 D. Kim, Y. Kim, K. Choi, J. C. Grunlan and C. Yu, *ACS Nano*, 2010, **4**, 513–523.
- 68 C. Yu, K. Choi, L. Yin and J. C. Grunlan, *ACS Nano*, 2011, **5**, 7885–7892.
- 69 S. L. Kim, K. Choi, A. Tazebay and C. Yu, *ACS Nano*, 2014, **8**, 2377–2386.
- 70 L. M. Veca, M. J. Mezziani, W. Wang, X. Wang, F. Lu, P. Zhang, Y. Lin, R. Fee, J. W. Connell and Y.-P. Sun, *Adv. Mater.*, 2009, **21**, 2088–2092.
- 71 L. Wang, Q. Yao, H. Bi, F. Huang, Q. Wang and L. Chen, *J. Mater. Chem. A*, 2014, **2**, 11107–11113.
- 72 W. Zheng, P. Bi, H. Kang, W. Wei, F. Liu, J. Shi, L. Peng, Z. Wang and R. Xiong, *Appl. Phys. Lett.*, 2014, **105**, 023901.
- 73 B. Zhang, J. Sun, H. E. Katz, F. Fang and R. L. Opila, *ACS Appl. Mater. Interfaces*, 2010, **2**, 3170–3178.
- 74 Y. Wang, K. Cai and X. Yao, *ACS Appl. Mater. Interfaces*, 2011, **3**, 1163–1166.
- 75 K. C. See, J. P. Feser, C. E. Chen, A. Majumdar, J. J. Urban and R. A. Segalman, *Nano Lett.*, 2010, **10**, 4664–4667.
- 76 N. E. Coates, S. K. Yee, B. McCulloch, K. C. See, A. Majumdar, R. A. Segalman and J. J. Urban, *Adv. Mater.*, 2013, **25**, 1629–1633.
- 77 S. Ma, K. Anderson, L. Guo, A. Yousuf, E. C. Ellingsworth, C. Vajner, H.-T. Wang and G. Szulczewski, *Appl. Phys. Lett.*, 2014, **105**, 073905.
- 78 B. Kim, H. Shin, T. Park, H. Lim and E. Kim, *Adv. Mater.*, 2013, **25**, 5483–5489.
- 79 Y. Zhang, J. Fang, C. He, H. Yan, Z. Wei and Y. Li, *J. Phys. Chem. C*, 2013, **117**, 24685–24691.
- 80 L. Groenendaal, F. Jonas, D. Freitag, H. Pielartzik and J. R. Reynolds, *Adv. Mater.*, 2000, **12**, 481–494.
- 81 Y.-F. Liu, J. Feng, Y.-F. Zhang, H.-F. Cui, D. Yin, Y.-G. Bi, J.-F. Song, Q.-D. Chen and H.-B. Sun, *Org. Electron.*, 2014, **15**, 2661–2666.
- 82 A. R. Cho, E. H. Kim, S. Y. Parka and L. S. Parkc, *Synth. Met.*, 2014, **193**, 77–80.
- 83 J. V. Li, A. M. Nardes, Z. Liang, S. E. Shaheen, B. A. Gregg and D. H. Levi, *Org. Electron.*, 2011, **12**, 1879–1885.
- 84 G. Garcia-Belmonte, P. P. Boix, J. Bisquert, M. Sessolo and H. J. Bolink, *Sol. Energy Mater. Sol. Cells*, 2010, **94**, 366–375.
- 85 Y. He and G. Galli, *Chem. Mater.*, 2014, **26**, 5394–5400.